

# Effect of Radiation, Absorption, Thermal radiation on Hydromagnetic mixed convective squeezing three dimensional flow of a nano fluid in a rotating channel with heat sources.

<sup>1</sup>Dr. M. Gayathri

<sup>1</sup>Assistant Professor of Mathematics

<sup>1</sup>Government First Grade College, Varthur, Bangalore-87

**Abstract** - An attempt has been to analyse the combined influence of thermo-diffusion, thermal radiation, on convective squeezing flow of a nanofluid in a rotating channel in the presence of heat source. By employing fourth-fifth order Runge-Kutta-Fehlberg scheme with the help of Maple, the non-linear equations have been solved. The effect of radiation, Soret effect, Heat source, rotation on velocity, temperature and concentration are exhibited through graphs. The stress, Nusselt and Sherwood number on the walls are evaluated numerically for different variations. It is found that an increase in Hall parameter enhances the velocities, reduces the temperature and concentration. The axial velocity reduces in the region (0,0.5) and enhances in (0.6,1.0) with increase in Soret parameter (Sr), radiation absorption(Q1) and nanoparticle volume fraction. The temperature and concentration reduces with Sr, Q1 and nanoparticle volume fraction.

**keywords** - Nanofluid, Radiation, Thermal Radiation, Absorption, Squeezing, Heat source, Hall effect.

## 1. INTRODUCTION:

The inspiration of suspended nanoparticles in a base fluid to increase the thermal conductivity was proposed by Choi [6] about a decade ago. Thereafter, theoretical and experimental investigations on the nanofluid heat transfer property have been conducted by Wang et al. [40], Eastman et al. [9], Buongiorno [5], etc. They have concluded that the thermal conductivity of the base fluid can be dramatically enhanced in the presence of nanoparticles. Besides, there are two models are available to incorporate nanoparticle effect on fluid flow problems namely single phase model and two-phase model. Further, Buongiorno or Tiwari and Das model is used to model the single-phase nanofluid. Two important mechanisms such as Brownian motion and thermophoresis are treated in Buongiorno model. However, in Tiwari and Das model, the effective fluid properties are taken into account. The nanofluids have tremendous applications such as engine cooling, solar water heating, cooling of electronic equipments, cooling of transformer oil, cooling of heat exchanging devices, in chillers, refrigerator-freezers, nuclear reactors, and space vehicles, due to their higher thermal conductivity and convective heat transfer rates.

Rotating flows of nanofluids have also garnered considerable attention. Such studies invoke Coriolis body force terms due to the rotation of the nanofluid (Mahajan and Arora [20]) considered convective instability in a thin layer of a rotating magnetic nanofluid, considering Brownian diffusion, thermophoresis and magnetophoresis effects. Using a Chebyshev pseudo spectral numerical method and considering different boundary conditions, they found that for water and ester based magnetic nanofluids, the magnetic field dominates the buoyancy mechanism in fluid layers about 1 mm thickness (Nadeem and Saleem [26]) is investigated with a homotopy analysis method (HAM) the transient mixed magnetohydrodynamic rotating nanofluid convection on a rotating cone with magnetic field, and considered three different cases where the fluid is rotating and the cone is at rest, the fluid and the cone are rotating with equal angular velocity in the same direction and where only the cone is in rotation. Beg et al. [4] analyzed the transient stagnation-point boundary layer flow of nanofluids from a spinning sphere, using both homotopy and Adomian decomposition methods. Rana et al. [27] studied with a variational finite element algorithm, the transient magneto-hydrodynamic boundary layer flow and heat transfer in an incompressible rotating nanofluid over a stretching continuous sheet, showing that both primary and secondary velocity are strongly retarded with increasing Hartmann (magnetic) number whereas temperature and nanoparticle concentration are enhanced. They also found that greater rotational parameter decelerates both primary and secondary velocity, and reduces temperature and nanoparticle concentration. Sheikholeslami et al. [28] used a fourth-order Runge-Kutta method to study magnetohydrodynamic (MHD) nanofluid flow and heat transfer in a rotating parallel plate channel system, considering copper, silver, alumina and titanium oxide nano-particles suspended in water. Hamad and Pop [12] also examined rotating hydromagnetic nanofluid convection from a permeable plate, noting that with increasing rotation and heat source parameters, the skin friction is reduced as is the temperature and thermal boundary layer thickness.

Recently, Sheikholeslami and Ganji [32] studied the MHD effects on nanofluid flow in a permeable channel. Kuznetsov and Nield [20] critically analyzed the natural convection flow of a nanofluid past a vertical plate. The problem of transient MHD free convection flow of a nanofluid over a rotating vertical plate is addressed by Hamad and Pop [12]. They solved the governing equations analytically using the perturbation method and found that, the inclusion of nanoparticles into the base fluid is capable of varying the flow pattern. Turkyilmazoglu [34] reported the exact solution for heat and mass transfer of magnetohydrodynamic

flow of nanofluid. Further, Turkyilmazoglu and Pop [35] have examined the heat and mass transfer of unsteady natural convection flow of nanofluid past a vertical infinite plate with thermal radiation. Das [7] discussed the problem of free convection flow of nanofluid bounded by moving vertical plate with constant heat source and convective boundary condition in a rotating frame of reference. He found that, the skin friction coefficient increases with an increase in the nanoparticle volume fraction. Recently, Sheikholeslami and Ganji [29] have presented the heat and mass transfer behaviour of unsteady flow of nanofluid between parallel plates in the presence of thermal radiation. They conclude that, the solutal boundary layer thickness increases with increase in radiation parameter.

When heat and mass transfer occur simultaneously in a moving fluid, the relation between the fluxes and the driving potentials are of more intricate nature. Mass fluxes can be created by temperature gradients and this is the Soret effect or thermo-diffusion effect. Adrian Postelnicu [1] has studied thermo-diffusion and diffusion thermo effects on combined heat and mass transfer through a porous medium under different conditions. Sreevani et. al. [31] has studied the unsteady free convective heat and mass transfer flow through porous medium dissipative effect in rotating channel. All the above mentioned studies are based on the hypothesis that the effect of dissipation is neglected. This is possible in case of ordinary fluid flow like air and water under gravitational force. But this effect is expected to be relevant for fluids with high values of the dynamic viscosity force. On the other hand, Barletta [3] and Zanchini [37] pointed out that relevant effects of viscous dissipation on the temperature profiles and the Nusselt number may occur in the fully developed convection in tubes. In view of this, several authors, notably, Muthu kumaraswamy et. al. [24] have studied the rotation effects on flow past an accelerated isothermal vertical plate with chemical reaction of first order. Jafarunnisa [16] has discussed the effect of thermal radiation and thermo diffusion on unsteady convective heat and mass transfer flow in the rotating system with heat sources. Alam et. al. [2] have discussed the steady MHD combined heat and mass transfer flow through a porous medium past an infinite vertical plate with viscous dissipation and joule heating effects in a rotating system. Srirangavani et al [30] has considered the effect of thermo-diffusion on convective heat and mass transfer flow with radiation absorption. Jayasudha [17] has discussed combined influence of thermo-diffusion and radiation absorption on convective heat and mass transfer flow past a stretching sheet with constant wall heat and mass transfer. Madhavilatha et al [19] have discussed the effect of non-linear density-temperature and concentration on rotating convective heat and mass transfer fluid flow past a porous stretching sheet with Soret and Dufour effects. Sukanya et al [33] have discussed combined influence of Hall Currents and Soret effect on convective heat and mass transfer flow past vertical porous stretching plate in rotating fluid and dissipation with constant heat and mass flux and partial slip.

On the other hand, an unsteady squeezing flow of an electrically conducting fluid occurs in many engineering and industrial applications such as lubrication, food industries, transient loading of mechanical components, power transmission, polymer processing, compression and injection modelling. The squeezing flow of a fluid was first introduced by Stefan [32], Following this work, many researchers have investigated such flow with different aspects. Numerical solution for a fluid film squeezed between two parallel plane surfaces have been reported by Hamza and Macdonald [14]. Domairry and Aziz [8] studied the squeezing flow of viscous fluid between parallel disks with suction or blowing analytically. Heat and mass transfer in the unsteady squeezing flow between parallel plates is analyzed by Mustafa et al [24], Hamza [13] discussed the effect of suction and injection on the squeezing flow between parallel plates. It is noted that very little attention has been given to study the three-dimensional flow in a rotating channel. Munawar et al [23] studied the three-dimensional flow in a rotating channel of lower stretching sheet in the presence of MHD effects. The mathematical equations are modelled with the help of Navier-Stokes equation and then they are solved numerically. Hayat et al [15] have discussed an unsteady mixed convection three-dimensional squeezing flow of an incompressible Newtonian fluid between two vertical parallel planes. Mahanthesh et al [21] have studied mixed MHD convection squeezing three-dimensional flow in a rotating channel filled with nanofluid.

Freidoonimehr et al. [10] presented the analytical solution for three-dimensional squeezing nanofluid flow in a rotating channel using Tiwari and Das model. With the aid of same model Gireesha et al. [11] have studied the effect of nanoparticles on flow and heat transfer of dusty fluid. Das [7] have found that the volume fraction parameter decreases the rate of heat transfer in a fully developed mixed convection flow through a vertical channel filled with water based nanofluid with the uniform transverse magnetic field.

The main objective of the present investigation is to study MHD effects on the three dimensional squeezing flow of an electrically conducting in a rotating channel and its heat and mass transfer characteristics. To the best of author's knowledge, such study has not received attention in the engineering sciences literature thus far. The governing equations are reduced to set of ordinary differential equations and then numerically solved by employing Runge-Kutta-Fehlberg fourth-fifth order method. Effect of pertinent parameters on velocity, temperature and concentration fields is examined through the plots. Skin-friction coefficients, Nusselt number and Sherwood number for different variations are studied numerically. The author have hope that the results obtained in the present study not only provide useful information for applications, it also serves as a complement to the previous studies.

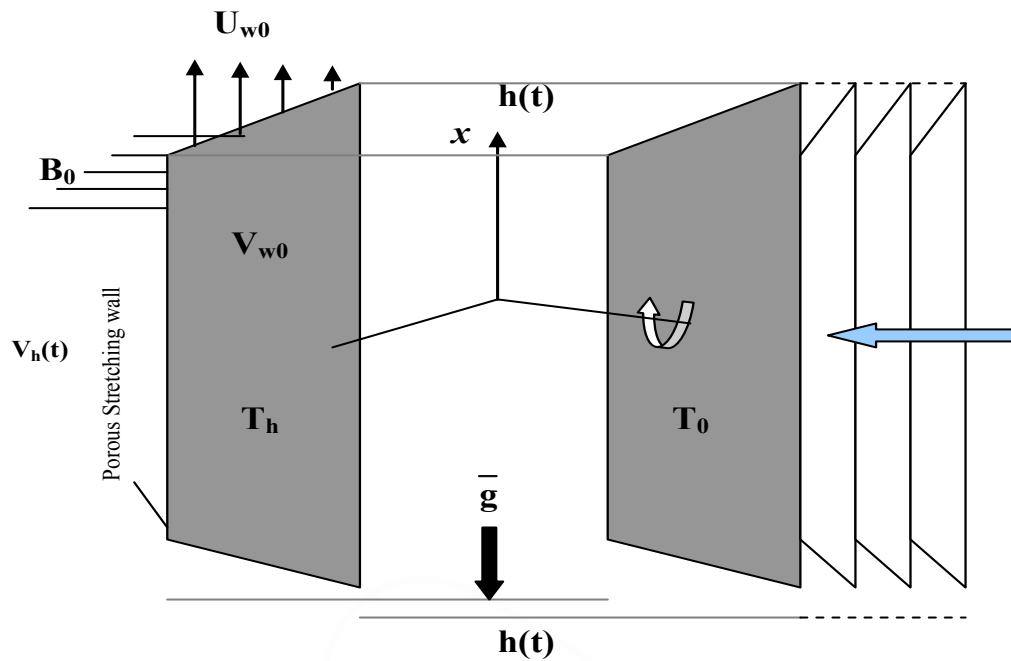


**Fig. 1 : Flow configuration and Coordinate system**

**2. MATHEMATICAL FORMULATION**

Consider an unsteady three-dimensional squeezing flow of an electrically conducting incompressible nanofluid in a vertical rotating channel. The plane positioned at  $y = 0$  is stretched with velocity  $U_{wo} = \frac{\alpha x}{(1 - \alpha t)}$  in  $X$ -direction and maintained at the constant temperature  $T_0$  and concentration  $C_0$ . The temperature at the other plane is  $T_h$  and located at a variable distance  $h(t) = \sqrt{v_f(1 - \alpha t)}$ . In negative  $Y$ -direction, the fluid is squeezed with a time dependent velocity  $V_h = \frac{dh}{dt} = -\frac{\alpha}{2} \sqrt{\frac{v_f}{\alpha(1 - \alpha t)}}$ . The fluid and the channel are rotated about  $y$ -axis with angular velocity  $\vec{\Omega} = \frac{\omega \hat{j}}{1 - \alpha t}$ . The transverse magnetic field is assumed to be variable kind  $\vec{B} = \frac{B_0}{\sqrt{(1 - \alpha t)}}$  and it is applied along  $y$ -axis. The fluid is sucked/injected from the plane located at  $y = 0$  as shown in figure 1. The magnetic Reynolds number is assumed to be small thus induced magnetic field is negligible. In addition, effects of Hall current, viscous dissipation and Joule heating are neglected.

Under those assumptions, the governing equations for the velocity and temperature fields in the presence of internal heating source/sink are given by [Hayat et al [15], Munawar et al [23]].

$$\frac{\partial u}{\partial x} + \frac{\partial v}{\partial y} = 0 \tag{1}$$

$$\frac{\partial u}{\partial t} + u \frac{\partial u}{\partial x} + v \frac{\partial u}{\partial y} + 2 \frac{\omega}{1 - \alpha t} w = -\frac{1}{\rho n f} \frac{\partial p}{\partial x} + v_{nf} \left( \frac{\partial^2 u}{\partial x^2} + \frac{\partial^2 u}{\partial y^2} \right) - \frac{\sigma B_0^2}{\rho n f (1 - \alpha t)} (u - mw) + \frac{g(\rho\beta)_{nf}}{\rho n f} (T - T_0) \tag{2}$$

$$\frac{\partial v}{\partial t} + u \frac{\partial v}{\partial x} + v \frac{\partial v}{\partial y} = -\frac{1}{\rho n f} \frac{\partial p}{\partial y} + v_{nf} \left( \frac{\partial^2 v}{\partial x^2} + \frac{\partial^2 v}{\partial y^2} \right) \tag{3}$$

$$\frac{\partial w}{\partial t} + u \frac{\partial w}{\partial x} + v \frac{\partial w}{\partial y} - 2 \frac{\omega}{1 - \alpha t} u = \nu_{rf} \left( \frac{\partial^2 w}{\partial x^2} + \frac{\partial^2 w}{\partial y^2} \right) - \frac{\sigma B_0^2}{\rho n_f (1 - \alpha t)} (mu - w) \tag{4}$$

$$\frac{\partial T}{\partial t} + u \frac{\partial T}{\partial x} + v \frac{\partial T}{\partial y} = \frac{k_{nf}}{(\rho C_p)_{nf}} \left( \frac{\partial^2 T}{\partial x^2} + \frac{\partial^2 T}{\partial y^2} \right) + \frac{Q_0}{(\rho C_p)_{nf} (1 - \alpha t)} (T - T_0) - \frac{1}{(\rho C_p)_{nf}} \frac{\partial(q_R)}{\partial y} \tag{5}$$

$$\frac{\partial C}{\partial t} + u \frac{\partial C}{\partial x} + v \frac{\partial C}{\partial y} = D_m \left( \frac{\partial^2 C}{\partial x^2} + \frac{\partial^2 C}{\partial y^2} \right) - \frac{k_c}{(1 - \alpha t)} (C - C_0) \tag{6}$$

where  $u, v$  and  $w$  are velocity components along  $X, Y$  and  $Z$  directions respectively,  $p$  is pressure,  $B_0$  is the magnetic field,  $\sigma$  is the electrical conductivity,  $g$  is the magnitude of acceleration due to gravity,  $\alpha$  is characteristic parameter with the dimension of reciprocal of time  $t$  and  $\alpha t < 1$ .  $T$  is temperature of the fluid  $Q_0$  is uniform volumetric heat generation/ absorption, here  $Q_0 < 0$  and  $Q_0 > 0$  are respectively corresponds to internal heat absorption and generation,  $\rho_{nf}$  is effective density of the nanofluid,  $\nu_{nf} = \frac{\mu_{nf}}{\rho_{nf}}$  is effective kinematic viscosity of the nanofluid,  $k_{nf}$  and  $(\rho C_p)_{nf}$  are effective thermal conductivity and

heat capacity of the nanofluid respectively. They are defined as follows:

$$\begin{aligned} \rho_{nf} &= (1 - \phi) \rho_f + \phi \rho_s \\ (\rho\beta)_{nf} &= (1 - \phi)(\rho\beta)_f + \phi(\rho\beta)_s \\ (\rho C_p)_{nf} &= (1 - \phi)(\rho C_p)_f + \phi(\rho C_p)_s \\ \mu_{nf} &= \frac{\mu_f}{(1 - \phi)^{2.5}} \\ \frac{k_{nf}}{k_f} &= \frac{(k_s + 2k_f) - 2\phi(k_f - k_s)}{(k_s + 2k_f) + 2\phi(k_f - k_s)} \end{aligned} \tag{7}$$

hence  $\phi$  is the solid volume fraction of the nanofluid,  $\rho_f$  is the density of base fluid,  $\rho_s$  is the density of the nanoparticle,  $\mu_f$  is the dynamic viscosity of the base fluid,  $(\rho C_p)_f$  is the heat capacity of the base fluid,  $(\rho C_p)_s$  is the heat capacity of the nanoparticle,  $k_f$  is the thermal conductivity of the base fluid and  $k_s$  is the thermal conductivity of nanoparticles.

The approximate boundary conditions for the present problem are

$$\left. \begin{aligned} u(x, y, t) &= U_{w0}, & v(x, y, t) &= V_{w0}, \\ w(x, y, t) &= 0, & T(x, y, t) &= T_0, C(x, y, t) = C_0 \end{aligned} \right|_{\text{at } y=0} \tag{8}$$

$$\left. \begin{aligned} u(x, y, t) &= 0, & v(x, y, t) &= V_h, \\ w(x, y, t) &= 0, & T(x, y, t) &= T_h, C(x, y, t) = C_h \end{aligned} \right|_{\text{at } y=h(t)} \tag{9}$$

Where  $T_h = T_0 + \frac{T_0}{1 - \alpha t}$ ,  $C_h = C_0 + \frac{C_0}{(1 - \alpha t)}$ ,  $V_{w0} = \frac{-V_0}{(1 - \alpha t)}$ .

Here  $V_0$  is constant,  $V_{w0} < 0$  corresponds injection whereas  $V_{w0} > 0$  corresponds wall suction.

To reduce the governing equations into a set of similarity equations, introduce the following similarity transformations [Munawar et al [22]].

$$\psi = \sqrt{\frac{\alpha \nu_f}{1 - \alpha t}} x f(\eta), \quad \eta = \frac{y}{h(t)}, \quad T = T_0 + \frac{T_0}{1 - \alpha t} \theta(\eta), \quad C = C_0 + \frac{C_0}{1 - \alpha t} C(\eta), \tag{10}$$

$$u = U_{w0} f_\eta \eta, \quad v = -\sqrt{\frac{\alpha \nu_f}{1 - \alpha t}} f(\eta), \quad w = U_{w0} g(\eta)$$

where a suffix  $\eta$  denote the differentiation with respect to  $\eta$  and  $\nu_f$  is the kinematic viscosity of the base fluid. Using the above transformations (10), the equation (1) is automatically satisfied, while the equation (2) – (6) are respectively reduces to the following nonlinear ordinary differential equations

$$f_{\eta\eta\eta} = \frac{\nu_f}{\nu_{nf}} \left[ f f_{\eta\eta} - f_{\eta}^2 - \beta \left( f_{\eta} \frac{\eta}{2} f_{\eta\eta} \right) - 2Rg - \frac{\rho_f}{\rho_{nf}} \frac{M^2}{1+m^2} (f_{\eta} - mg_{\eta}) + \frac{(\rho\beta)_{nf}}{\rho_{nf}} Gr_m \theta \right] = \frac{(1-\alpha t)^2 \nu_f}{\rho_{nf} \nu_{nf} a^2 x} \frac{\partial p}{\partial x} \tag{11}$$

$$f_{\eta\eta} - \frac{\nu_f}{\nu_{nf}} \left[ -f f_{\eta} + \frac{\beta}{2} (f + \eta f_{\eta}) \right] = -\frac{1-\alpha t}{\rho_{nf} \nu_{nf} a} p_{\eta} \tag{12}$$

$$g_{\eta\eta} + \frac{\nu_f}{\nu_{nf}} \left[ f g_{\eta} - f_{\eta} g - \beta \left( g \frac{\eta}{2} g_{\eta} \right) + 2Rf_{\eta} \right] - \frac{\rho_f}{\rho_{nf}} \frac{M^2}{1+m^2} (mf_{\eta} - g) = 0 \tag{13}$$

$$\left( 1 + \frac{4Rd}{3} \right) \theta_{\eta\eta} + \frac{k_f}{k_{nf}} Pr \left[ \left( 1 - \phi + \frac{\phi(\rho C_p)_s}{(\rho C_p)_f} \right) \left\{ \beta \left( \theta + \frac{\eta}{2} \theta_{\eta} \right) + f \theta_{\eta} \right\} - Q \theta \right] = 0. \tag{14}$$

$$C_{\eta\eta} + Sc \left[ \left\{ \beta \left( C + \frac{\eta}{2} C_{\eta} \right) + f C_{\eta} \right\} - \gamma C \right] = 0 \tag{15}$$

Reduced boundary conditions are;

$$\begin{aligned} f_{\eta} = 1, \quad f = S, \quad g = 0, \quad \theta = 0, \quad C = 0 \quad \text{at} \quad \eta = 0 \\ f_{\eta} = 0, \quad f = \frac{\beta}{2}, \quad g = 0, \quad \theta = 1, \quad C = 1 \quad \text{at} \quad \eta = 1 \end{aligned} \tag{16}$$

where

- $\beta = \alpha/a$  is the squeezing parameter,
- $R = \omega/\alpha$  is rotation parameter,
- $M^2 = \sigma B_0^2 / \alpha \rho_f$  is magnetic parameter,
- $Gr_m = Gr / Re^2$  is mixed convection parameter,
- $Gr = g \beta_f T_0 x^3 / \nu_f^2 (1-\alpha t)$  is modified Grashaf number,
- $Re = x U_{w0} / \nu_f$  is Reynolds number,
- $Pr = (\mu c_p)_f / k_f$  is the Prandtl number,
- $Q = Q_0 / \alpha (\rho C_p)_f$  is heat source / sink parameter and
- $S = V_{w0} / \alpha h$  is suction / injection parameter.

$$Sc = \frac{\nu_f}{D_m} \text{ is the Schmidt number}$$

$$Sr = \frac{D_m K_T T_0}{a T_m C_0} \text{ is the Soret parameter}$$

$$\gamma = \frac{kc}{a} \text{ is the chemical reaction parameter}$$

$$Q = Q_0 / \alpha (\rho C_p)_f \text{ is heat source / sink parameter}$$

It is important to mention that,  $\beta = 0$  represents plates are stationary,  $\beta > 0$  corresponds to the plate which is located at  $y = h(t)$  moves towards the plate which is located at  $y = 0$  and  $\beta < 0$  corresponds to the plate at  $y = y(t)$  moves apart with respect to the plate at  $y = 0$ .

Now in order to reduce the number of independent variables by cross differentiation, the set of equations (11) - (14) takes the following form:

$$\begin{aligned} f_{\eta\eta\eta} - (1-\phi)^{2.5} \left( 1 - \phi + \phi \frac{\rho_s}{\rho_f} \right) \left[ \frac{\beta}{2} (3 f_{\eta\eta} + \eta f_{\eta\eta\eta}) f_{\eta} f_{\eta\eta} - f f_{\eta\eta\eta} + 2Rg_{\eta} \right] \\ - (1-\phi)^{2.5} \frac{M^2}{1+m^2} (f_{\eta\eta} - mg_{\eta}) + (1-\phi)^{2.5} \left( 1 - \phi + \frac{(\rho\beta)_s}{(\rho\beta)_f} \right) G \theta_{\eta} = 0 \end{aligned} \tag{17}$$

$$g_{\eta\eta} + (1-\phi)^{2.5} \left( 1 - \phi + \phi \frac{\rho_s}{\rho_f} \right) \left[ f g_{\eta} - f_{\eta} g - \beta \left( g + \frac{\eta}{2} g_{\eta} \right) + 2R f_{\eta} \right] - (1-\phi)^{2.5} \frac{M^2}{1+m^2} (m f_{\eta} - g) = 0 \tag{18}$$

$$\frac{(k_s + 2k_f) - 2\phi(k_f - k_s)}{(k_s + 2k_f) + 2\phi(k_f - k_s)} \left( 1 + \frac{4Rd}{3} \right) \theta_{\eta\eta} - \text{Pr} \left( \left( 1 - \phi + \frac{\phi(\rho C_p)_s}{(\rho C_p)_f} \right) \left\{ \beta \left( \theta + \frac{\eta}{2} \theta_{\eta} \right) + f \theta_{\eta} \right\} - Q \theta \right) = 0 \tag{19}$$

$$C_{\eta\eta} - Sc \left( \left\{ \beta \left( C + \frac{\eta}{2} C_{\eta} \right) + f C_{\eta} \right\} - \gamma C \right) = 0 \tag{20}$$

For engineering and industrial point of view, one has usually less interest in velocity and temperature profiles nature than in the value of the skin-friction and rate of heat transfer. Therefore expression for the local skin-friction coefficient and the local Nusselt number at both the walls are defined as;

$$C_{f, \text{ at } y=0}^* = \frac{(\tau_{xy})_{y=0}}{\rho_{nf} U_{w0}^2}, \quad C_{f, \text{ at } y=h(t)}^* = \frac{(\tau_{xy})_{y=h(t)}}{\rho_{nf} U_{w0}^2}, \tag{21}$$

$$Nu_{\text{ at } y=0}^* = \sqrt{\frac{v_f}{a}} \frac{(q_{xy})_{y=0}}{k_f T_0}, \quad Nu_{\text{ at } y=h(t)}^* = \sqrt{\frac{v_f}{a}} \frac{(q_{xy})_{y=h(t)}}{k_f T_0}, \tag{22}$$

where  $\tau_{xy}$  is the shear stress and  $q_{xy}$  is the heat flux, which are given by

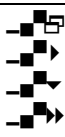
$$\tau_{xt} = \mu_{nf} \left( \frac{\partial u}{\partial x} + \frac{\partial u}{\partial y} \right) \quad \text{and} \quad q_{xt} = -k_{nf} \left( \frac{\partial T}{\partial x} + \frac{\partial T}{\partial y} \right) \tag{23}$$

In view of equation (22) and similarity transformations (10) equations (21) & (22) will takes the following form:

$$\begin{aligned} C_{f, \text{ at } y=0}^* &= \sqrt{Re} & C_{f, \text{ at } y=0}^* &= f_{\eta\eta}(0) / (1-\phi)^{2.5} \left( 1 - \phi + \phi \left( \frac{\rho_s}{\rho_f} \right) \right) \\ C_{f, \text{ at } y=h(t)}^* &= \sqrt{Re} & C_{f, \text{ at } y=h(t)}^* &= f_{\eta\eta}(1) / (1-\phi)^{2.5} \left( 1 - \phi + \phi \left( \frac{\rho_s}{\rho_f} \right) \right) \\ Nu_{\text{ at } y=0} &= (1-\alpha t)^{1.5} & Nu_{\text{ at } y=0}^* &= -\frac{k_{nf}}{k_f} \theta_{\eta}(0), \\ Nu_{\text{ at } y=h(t)} &= (1-\alpha t)^{1.5} & Nu_{\text{ at } y=h(t)}^* &= -\frac{k_{nf}}{k_f} \theta_{\eta}(1) \\ Sh_{\text{ at } y=0} &= (1-\alpha t)^{1.5} & Sh_{\text{ at } y=0}^* &= -C_{\eta}(0), \\ Sh_{\text{ at } y=h(t)} &= (1-\alpha t)^{1.5} & Sh_{\text{ at } y=h(t)}^* &= -C_{\eta}(1) \end{aligned} \tag{24}$$

**Table 1 :** In the absence of Hall effects(m=0) the results are in good agreement with Mahantesh et al(21)

| Parameters |     |         | Mahantesh et al(21) |          |         |         | Present results |          |         |   |
|------------|-----|---------|---------------------|----------|---------|---------|-----------------|----------|---------|---|
| R          | 0.5 | 4.34299 | 0.277668            | -        | -       | 4.34293 | 0.277666        | -        | -       |   |
|            | 1.0 |         |                     | 0.99998  | 1.31302 |         |                 | 0.99998  | 1.31300 |   |
|            | 1.5 | 4.30684 | 0.833542            | -        | -       | 4.30686 | 0.833541        | -        | -       |   |
|            | 2.0 |         |                     | 0.99998  | 1.31305 |         |                 | 0.99998  | 1.31303 |   |
|            |     |         | 4.23431             | 1.391062 | -       | -       | 4.23434         | 1.391063 | -       | - |
|            |     | 4.12494 | 1.951422            | -        | -       | 4.12496 | 1.951426        | -        | -       |   |
|            |     |         |                     | 0.99999  | 1.31311 |         |                 | 0.99999  | 1.31309 |   |
| Nr         | 0.5 | 4.34299 | 0.277668            | -        | -       | 4.34297 | 0.277665        | -        | -       |   |
|            | 1.5 |         |                     | 0.99996  | 1.31302 |         |                 | 0.99998  | 1.31301 |   |
|            | 3.5 | 4.34302 | 0.277667            | -1.0004  | -       | 4.34300 | 0.277663        | -        | -       |   |
|            | 5.0 |         |                     |          | 1.31368 |         |                 | 1.00044  | 1.31366 |   |
|            |     |         |                     |          |         |         |                 |          |         |   |

|         |   |         |          |         |         |         |          |         |         |         |
|---------|---|---------|----------|---------|---------|---------|----------|---------|---------|---------|
|         |   | 4.34305 | 0.277665 | -       | -       | 4.34304 | 0.277662 | -       | -       |         |
|         |   |         | 1.00088  | 1.31431 |         |         |          | 1.00083 | 1.31430 |         |
|         |   | 4.34313 | 0.277662 | -       | -       | 4.34316 | 0.277659 | -       | -       |         |
|         |   |         | 1.00219  | 1.31595 |         |         |          | 1.00212 | 1.31594 |         |
| $\beta$ |  | 4.34299 | 0.277668 | -       | -       | 4.34296 | 0.277666 | -       | -       |         |
|         |   |         |          | 0.99998 | 1.31302 |         |          |         | 0.99998 | 1.31300 |
|         |   | 3.67161 | 0.225586 | -       | -       | 3.67159 | 0.225580 | -       | -       |         |
|         |   |         |          | 0.99997 | 1.36765 |         |          |         | 0.99997 | 1.36765 |
|         |   | 3.03904 | 0.177955 | -       | -       | 3.03902 | 0.177956 | -       | -       |         |
|         |   |         |          | 0.99997 | 1.42139 |         |          | 0.99997 | 1.42136 |         |
|         |   | 2.41319 | 0.132139 | -       | -       | 2.41313 | 0.132135 | -       | -       |         |
|         |   |         |          | 0.99996 | 1.47682 |         |          | 0.99996 | 1.47679 |         |

### 3. NUMERICAL METHOD AND VALIDATION

A set of non-similar equations (15) - (17) are nonlinear in nature and possess no analytical solution thus a numerical treatment would be more appropriate. These set of ordinary differential equations together with the boundary conditions (16) are numerically solved by employing fourth-fifth order Runge-Kutta-Fehlberg scheme with the help of Maple. This algorithm in Maple is proven to be precise and accurate and which has been successfully used to solve a wide range of nonlinear problem in transport phenomena especially for flow and heat transfer problems. In this study, we set the relative error tolerance to  $10^{-6}$ . Comparison results are recorded in table 1 and are found to be in excellent agreement. The effects of development of the squeezing three-dimensional flow and heat transfer in a rotating channel utilizing nanofluid are studied for different values of squeezing parameter, rotation parameter, magnetic parameter, suction/injection parameter, mixed convection parameter, nanoparticle volume fraction parameter, Prandtl number, radiation parameter, Schmidt number, Chemical reaction parameter and heat source/sink parameter. In the following section, the results are discussed in detail with the aid of plotted graphs and tables.

Figs. 2a-2d are plotted for  $f'$ ,  $g$ ,  $\theta$  and  $C$  profiles against  $\eta$  for different values of  $G$  by fixing other parameters. Thermal Grashof number signifies the relative magnitude of the thermal buoyancy force and the opposing frictional force (viscous hydrodynamic force) acting on the nanofluids. It can be seen from the profiles that the temperature, concentration decrease with increase in Grashof number while the axial velocity  $f'$  enhances in the flow region (0.0,0.2), reduces in the region (0.2,0.5) and enhances in the region (0.5,1) and the transverse velocity  $g$  reduces in magnitude in the entire flow region (0,1.0). With increase in  $G$ . This may be attributed to the fact that an increase in  $G$  increases the thickness of the momentum boundary layer and decreases the thickness of the thermal and solutal boundary layer.

Figs. 3a-3d depict the effect of magnetic field parameter ( $M^2$ ) on  $f'$ ,  $g$ ,  $\theta$  and  $C$ . the parameter  $M$  is related directly to the applied magnetic field strength  $H_0$ . Increasing magnetic field strength therefore elevates the Lorentz drag force which inhibits  $f'$  in the region (0.2,0.5) and enhances in the remaining region. It can be found from the profiles that the transverse velocity component  $g$  decreases in magnitude with increase in  $M$  in the entire flow region (fig.3b), while the axial velocity  $f'$  reduces in the right half (0.2,0.5) and enhances in the left half (0.5,1.0) of the channel (fig.3a). Effectively the application of transverse magnetic field to the electrically conducting nanofluid generates a resistive type force, which acts against the motion of the nanofluid. The thickness of the thermal and solutal boundary layers decreases with increase in  $M$  which results in a fall in the temperature and concentration in the flow region (fig.3c & 3d). However the application of the magnetic field achieves excellent flow control in the regime and provides a simple but effective mechanism for regulating nanomaterials processing operation.

Figs.4a-4d illustrates the variation of  $f'$ ,  $g$ ,  $\theta$  and  $C$  with Hall parameter ( $m$ ). It can be seen from the profiles that the axial velocity component experience an enhancement in the flow region except in the region (0.2,0.5) where it reduces with increasing value of Hall parameter. This may be attributed to the fact that the thickness of the momentum boundary layer along  $X$  and  $Z$  directions reduces with Hall parameter (fig.4a&4b). An increase in  $m$  reduces the thickness of the thermal and solutal boundary layer which leads to a rise in the temperature and concentration depreciate in the flow region (figs.4c&4d).

The influence of rotation parameter ( $R$ ) on  $f'$ ,  $g$ ,  $\theta$  and  $C$  can be observed from the figs.5a-5d. The rotational parameter features in the Coriolice body force arising in both the dimensionless primary and secondary momentum equations (15&16). The axial velocity component enhances in the region (0,0.5) and reduces in (0.5,1.0) while the transverse velocity  $g$  increases with increase in  $R$ . The temperature and concentration distributions experience a reduction in the entire flow region with increase in rotation parameter ( $R$ ). This is due to the fact thickness of the thermal and solutal boundary layers decrease with  $R$ .

Figs.6a-6d are plotted to illustrate the effect of heat source parameter ( $Q$ ) on the flow variables. It can be seen from the profiles that the transverse velocity component ( $g$ ) enhances in the flow region with increase in the strength of the heat generating / absorbing source. This may be attributed to the fact that in the presence of heat generating /absorbing source, energy

is generated in the flow region. From fig.6a, we find that the axial velocity enhances in the region (0,0.5) and reduces in magnitude in the region(0.5,1.0) with increase in the strength of the heat generating source while it enhances with the strength of the heat absorbing source. From fig.6c&6d we find that in the presence of heat generating /absorbing source, energy is absorbed in the flow region, which results in a reduction in the temperature. The effect of heat source parameter(Q) on the concentration is to decrease C with Q in the entire flow region(fig.6d).

Figs.7a-7d show the influence of thermal radiation on  $f'$ ,  $g$ ,  $\theta$  and C. It can be seen from the profiles that there is a significant enhancement in the region (0,0.2) and depreciation in the magnitude of the velocity components  $f'$  in the region(0.2,0.5) while in the region(0.5,1.0) it enhances. The transverse velocity  $g$  experiences an enhancement in the entire flow region with increase in  $N_r$ . The radiation parameter is found to increase the hydrodynamic boundary layer along  $x$  and  $y$ -directions. The presence of the thermal radiation is very significant on the variation of temperature. It is seen that the temperature decreases rapidly in the presence of thermal radiation parameter throughout the flow region. This may be attributed to the fact that as the Roseland radioactive absorption parameter  $R^*$  diminishes the corresponding heat flux diverges and thus falling the rate of radiative heat transfer to the fluid causing a fall in the temperature of the fluid. The thickness of the thermal boundary layer also decreases with increase in  $R_d$  (fig.7c).The effect of mass concentration can be seen from fig.7d.We find a reduction in the concentration with a rise in  $R_d$ , owing to a fall in the thickness of the solutal boundary layer.

The effect of nanoparticle volume fraction ( $\phi$ ) on  $f'$ ,  $g$ ,  $\theta$  and C can be seen from the figs.8a-8d.As the volume fraction increases, the thermal conductivity of the nano-fluid is elevated. Therefore thermal diffusion is associated in the regime. It can be found from the profiles that an increase in nanoparticle volume fraction( $\phi$ ) leads to an enhancement in (0,0.2) and depreciation in the region(0.2,0.5) in the axial velocity component while the transverse velocity  $g$  increases with increase in  $\phi$ . This may be attributed to the fact that the thickness of the momentum boundary layer enhances with increase in  $\phi$ . Also the thickness of the thermal and solutal boundary layer decrease with increase in  $\phi$  which leads to a fall in temperature and concentration in the flow region(figs.8c&8d).

Figs.9a-9d present the typical profiles namely,  $f'$ ,  $g$ ,  $\theta$  and C respectively for different values of the squeezing parameter( $\beta$ ). From figs.8a-8d show that the magnitude of the axial velocity ( $f'$ ) increases in the region (0,0.2),reduces in the region (0.2,1.0)and transverse velocity ( $g$ ) is a decreasing function of the squeezing parameter( $\beta$ ). This implies that squeezing effect on flow field is accumulated by it An increase in  $\beta$  results in a reduction in the temperature and the nano-particle concentration (figs.8c&8d). This is due to the fact that a rise in squeezing parameter values leads to a decrease in the thickness of the thermal boundary layer and the solutal boundary layer thickness.

Figs.10a-10d illustrate the effect of suction /injection on the flow variables. It can be seen from the profiles that an increase in suction/injection parameter( $fw>0$ ,  $fw<0$ ) enhances the all the velocity components in the entire flow region (10a-10b).From figs.10c&10d we find that an increase in suction/injection parameter ( $fw>0/fw<0$ ) reduces the temperature and enhances the concentration in the entire flow region.

The effect of Schmidt number( $Sc$ ) on C is exhibited in fig.11d. From the profiles we find that there is a sustained reduction in the concentration magnitudes of nano-particle species with increasing Schmidt number. The Schmidt number represents the ratio of the momentum diffusivity to the mass (nano-particle species) diffusivity i.e., it relates the thickness of the hydrodynamic boundary layer to that of the concentration boundary layer. It also relates the momentum (viscous) diffusion rate to the molecular (nano-particle) diffusion rate. As  $Sc$  is increased the nano-particle molecular diffusivity is reduced. This results in decreasing species diffusion rates and a lowering of in nano-particle concentration magnitudes throughout the boundary layer. Physically this also manifests in a decrease in the nano-particle concentration boundary layer thickness with increasing Schmidt number. Also the axial velocity enhances while the transverse velocity reduces with increase in  $Sc$ (figs.11a&11b).

The effect of chemical reaction on C can be seen from fig.12a-12d.It can be see from the profiles that the concentration reduces in the degenerating chemical reaction case and enhances in the generating chemical reaction case. This amounts to the fact that the thickness of the solutal boundary layer decreases with  $\gamma > 0$  and increases with  $\gamma < 0$ . The thickness of the thermal boundary layer reduces with  $\gamma > 0$ and enhances with  $\gamma < 0$  (fig.12c). The axial velocity ( $f'$ ) reduces in the region (0,0.2) and enhances in (0.2,1.0) in the degenerating chemical reaction case while in the generating case, it enhances in entire flow region except in the region (0.2,0.5)where it reduces (fig.12a). From fig.12b we find that the transverse velocity ( $g$ ) reduces in the region (0,0.5) and enhances in (0.5,1.0)in the degenerating case while in generating case a reversed effect is noticed.

Fig.13a-13d illustrate the effect of radiation absorption ( $Q_1$ ) on  $f'$ ,  $g$ ,  $\theta$  and C. It can be seen from the profiles that the axial velocity enhances in the flow region except in (0.2,0.5)where it depreciates and the transverse velocity increases in magnitude with increase in  $Q_1$  in the entire flow region. From 13c&d we find that an increase in  $Q_1$  reduces the thickness of the thermal and solutal boundary layers which results in the depreciation of the temperature and concentration in the flow region(fig.13c&d)

The effect of Prandtl number( $Pr$ ) on  $f'$ ,  $g$ ,  $\theta$  and C can be seen from figs.14a-14d. Prandtl refers to the relative contribution of momentum diffusion to thermal diffusion in the boundary layer regime. Furthermore, an increase in Prandtl number results in a decrease in the temperature distribution in the thermal boundary layer. The physical reason is that smaller values of Prandtl number are associated with greater thermal conductivity, and therefore heat is able to diffuse away from the heated surface more rapidly than at higher values of Prandtl number i.e the energy diffusion rate is greater than the momentum



diffusion rate for Pr. Effectively the rate of heat transfer is reduced and an increase in Pr induces a reduction in the thickness of the thermal boundary layer. The effect of Prandtl number is to diminish the nano-particle concentration in the flow region (14d). From the profiles we find that the transverse velocity component experiences a depreciation with increase in Pr. The axial velocity ( $f'$ ) enhances in the flow region except in the region (0,0.25) where it reduces in magnitude. Also lesser the thermal diffusivity smaller the thickness of the thermal boundary layer while solutal boundary layer with increases in Pr in the entire flow region (figs. 14c&d).

The Skin friction components  $\tau_x, \tau_y$ , Nusselt number and Sherwood number on the walls ( $\eta = 0, 1$ ) are exhibited in tables.2 for different parametric variations. The skin friction component  $\tau_x$  reduces on both walls ( $\eta = 0 \& 1$ ) and while  $\tau_z$  enhances on  $\eta = 0$  and reduces on  $\eta = 1$  with increase in G. An increase in M enhances  $\tau_x$  on both the walls while  $\tau_z$  reduces on the left wall and enhances on the right wall. An increase in the Hall parameter (m) reduces  $\tau_x$  on both the walls while  $\tau_z$  increases with  $m \leq 1.0$  and reduces with higher  $m \geq 1.5$  on both walls. An increase in rotation parameter (R) reduces  $\tau_x$  and enhances  $\tau_z$  on  $\eta = 0 \& 1$ . With reference to nanoparticle volume fraction ( $\phi$ ) we find that  $\tau_x$  enhances and  $\tau_z$  reduces on the left wall and while they reduce on the right wall. Higher the radiative heat flux smaller the skin friction component  $\tau_x$  and enhances  $\tau_z$  on both the walls. The variation of skin friction components with heat source parameter (Q) shows that  $\tau_x$  enhances with increase in  $Q > 0$  and reduces with  $Q < 0$  on  $\eta = 0 \& 1$  while a reversed effect is observed in the behavior of  $\tau_z$  on the walls. With respect to chemical reaction parameter ( $\gamma$ ), we find that  $\tau_x$  reduces,  $\tau_z$  enhances in the degenerating chemical reaction case while in the generating case,  $\tau_x$  enhances,  $\tau_z$  reduces on the left wall. On the right wall,  $\tau_x$  enhances and  $\tau_z$  reduces on the right wall in both the degenerating and generating chemical reaction cases. An increase in the squeezing parameter ( $\beta$ ) smaller  $\tau_x$  and larger  $\tau_z$  on both the walls. With reference to suction parameter (fw) we find that  $\tau_x, \tau_z$  enhance at  $\eta = 0 \& 1$ , with increase in suction/injection parameter. Lesser the thermal diffusivity larger the skin friction component  $\tau_x$  and smaller  $\tau_z$  at  $\eta = 0$ , while  $\tau_x$  reduces and  $\tau_z$  enhances at  $\eta = 1$ . The variation of skin friction components with Prandtl number (Pr) illustrate that lesser the thermal diffusivity smaller the skin friction components at both the walls.

The rate of heat transfer (Nu) and mass transfer (Sh) at  $\eta = 0, 1$  are shown in table.2. The rate heat transfer enhances at the left and right walls with increase in G. An increase in M or R or Rd enhances Nu at the left wall and reduces at the right wall. An increase in  $Q > 0$ , enhances Nu at the left wall and reduces at the right wall while a reversed effect is noticed at the walls with increase in  $Q < 0$ . An increase in the suction parameter ( $fw > 0$ ) reduces Nu at the left wall and enhances at the right wall while a reversed effect is noticed in Nu with increase in  $fw < 0$ . The variation of Nu with squeezing parameter  $\beta$  shows that Nu increases at  $\eta = 0$  and decreases at  $\eta = 1$  with increasing  $\beta$ . With increase in nanoparticle volume fraction ( $\phi$ ) we notice an enhancement in the rate of heat transfer at both the walls. An increase in Prandtl number reduces Nu at  $\eta = 0$  and enhances at  $\eta = 1$ .

An increase in G or Pr enhances the rate of mass transfer (Sh) at the left wall ( $\eta = 0$ ) and reduces at the right wall ( $\eta = 1$ ). Sh reduces at both the walls with magnetic parameter (M). The rate of mass transfer reduces at  $\eta = 0$  and enhances at  $\eta = 1$  with increase in R. Sh reduces at  $\eta = 0$  and enhances at  $\eta = 1$  with increase in the strength of the heat generating source while in the case of heat absorbing source, the rate of mass transfer enhances at  $\eta = 0$  and reduces at  $\eta = 1$ . An increase in chemical reaction parameter ( $\gamma > 0$ ) enhances Sh at both the walls while in the case of generating case, it enhances at the left wall and reduces at the right wall. An increase in  $fw > 0$  reduces Sh at the left wall and enhances at the right wall while a reversed behaviour is noticed in Sh with  $fw < 0$ . The rate of mass transfer experiences an enhancement at both the walls with increases in nanoparticle volume fraction  $\phi$ , radiation parameter Rd. Sh reduces with Rotation parameter R and squeezing parameter  $\beta$  at the left wall while a reversed effect is noticed at the right wall.

## CONCLUSIONS:

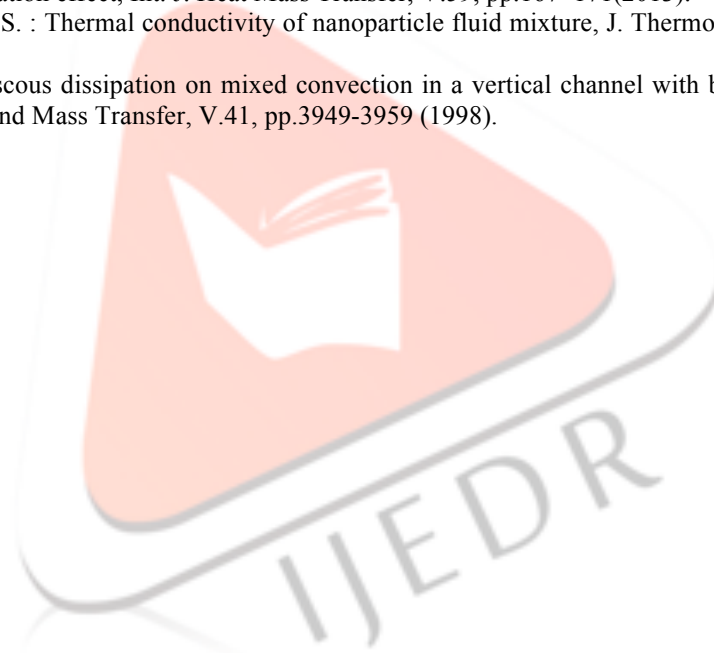
- 1) An increase in G reduces the axial velocity, enhances the transverse velocity, temperature and concentration. The skin friction components reduces at the  $\eta = 0$  and reduces at  $\eta = 1$ . An increase in G enhances Nu and Sh at  $\eta = 0$  while Nu enhances and Sh reduces at  $\eta = 1$ .
- 2) Higher the Lorentz force smaller the velocity components and larger the temperature and concentration, the skin friction enhances at the left wall and reduces at the right wall. Nu enhances and Sh reduces at  $\eta = 0$  while they reduces at  $\eta = 1$  with increase in M.
- 3) An increase in rotation parameter (R) enhances the axial velocity, temperature and concentration while the transverse velocity reduces. The skin friction reduces at  $\eta = 0$  and enhances at  $\eta = 1$ . Nu enhances and Sh reduces at  $\eta = 0$  while at  $\eta = 1$ , Nu reduces and Sh enhances.
- 4) An increase in nanoparticle volume concentration ( $\phi$ ) reduces the velocities and enhances the temperature and concentration. The skin friction enhances at  $\eta = 0$  and reduces at  $\eta = 1$ . The Sherwood number enhances at  $\eta = 0 \& 1$  with  $\phi$ .
- 5) Higher thermal radiation (Rd) smaller the axial velocity, temperature and larger the transverse velocity, concentration. The skin friction and Nusselt number enhances at  $\eta = 0$  and reduces at  $\eta = 1$ .
- 6) The concentration reduces in the degenerating chemical reaction and enhances in the generating case. Sh enhances at  $\eta = 0 \& 1$  with  $\gamma > 0$  while for  $\gamma < 0$ , sh enhances at  $\eta = 0$  and reduces at  $\eta = 1$ .
- 7) An increase in the squeezing parameter ( $\beta$ ) enhances the velocities, temperature and reduces the concentration. An increase in  $\beta$  reduces the skin friction, Sh and reduces Nu at  $\eta = 0$  while at  $\eta = 1$ ,  $\tau_x$  reduces and Sh enhances with  $\beta$ .

- 8) An increase in heat source parameter( $Q$ ) reduces the velocities, temperature and concentration. reduces with  $Q > 0$  and enhances with  $Q < 0$  at both the walls. The rate of heat transfer enhances with  $Q > 0$  and reduces with  $Q < 0$  at  $\eta=0$  while it reduces at  $\eta=1$  with increase in  $Q > 0$  and  $Q < 0$ .
- 9) The velocities enhances with increase in  $fw$ , The temperature and concentration reduces with  $fw > 0$  while for  $fw < 0$ , the temperature reduces and the concentration enhances in the flow region.

## REFERENCES

- [1] Adrian Postelnicu : Influence of magnetic field on heat and mass transfer by natural convection from vertical surfaces in porous media considering Soret and Dufour effects. *Int. J. of Heat and Mass Transfer*, V.47, pp.1467-1472 (2004).
- [2] Alam, Md, Delower Hossain, M and Arif Hossain, M : Viscous dissipation and joule heating effects on steady MHD combined heat and mass transfer flow through a porous medium in a rotating system. *Journal of Naval Architecture and Marine Engineering*, V.2, pp.105-120 (2011).
- [3] Barletta, A : Laminar mixed convection with viscous dissipation in a vertical channel. *Int. J. Heat Mass Transfer*, V.41, PP.3501-3513 (1998).
- [4] Beg OA, Mabood F and Nazrul Islam M. : Homotopy simulation of nonlinear unsteady rotating nanofluid flow from a spinning body. *International Journal of Engineering Mathematics* 2015; Article ID 272079, 15 pages, <http://dx.doi.org/10.1155/2015/272079>.
- [5] Buongiorno J. : Convective transport in nanofluids, *ASME J. Heat Transfer*, V.128, pp. 240–250(2006).
- [6] Choi S.U.S., Siginer D.A., Wang H.P. : Enhancing Thermal Conductivity of Fluids with Nanoparticles, *Developments and Applications of Non-Newtonian Flows*, The American Society of Mechanical Engineers, New York, FED-vol. 231/MDvol. 66, pp. 99–105 (1995).
- [7] Das K. : Flow and heat transfer characteristics of nanofluids in a rotating frame, *Alexandria Eng. J.*, 53 (3), pp.757–766(2014).
- [8] Domairry, G. and Aziz, A. (2009), “Approximate analysis of MHD squeeze flow between two parallel disks with suction or injection by homotopy perturbation method”, *Mathematical Problems in Engineering* , Vol. 2009. doi: 10.1155/2009/603916.
- [9] Eastman J.A., Choi S.U.S., Li S., Yu W., Thompson L.J. : Anomalous increased effective thermal conductivity of ethylene glycol-based nanofluids containing copper nanoparticles, *Appl. Phys. Lett.* V.78, pp. 718–720 (2001).
- [10] Freidoonimehr N., Rostami B, Rashidi M.M., Momoniat E. : Analytical modelling of three-dimensional squeezing nanofluid flow in a rotating channel on a lower stretching porous wall, *Math. Probl. Eng.*, 2014,14, 692728 (2014).
- [11] Gireesha B.J., Mahanthesh B., Gorla R.S.R. : Suspended particle effect on nanofluid boundary layer flow past a stretching surface, *J. Nanofluids*, V.3 (3), pp. 267–277 (2014).
- [12] Hamad M.A.A., Pop I. : Unsteady MHD free convection flow past a vertical permeable flat plate in a rotating frame of reference with constant heat source in a nanofluid, *Heat Mass Transfer*, V.47, pp.1517–1524 (2011).
- [13] Hamza, E.A. (1999), “Suction and injection effects on a similar flow between parallel plates”, *Journal of Physics D: Applied Physics* , Vol. 32 No. 6, pp. 656-663.
- [14] Hamza, E.A. and Macdonald, D.A. (1981), “A fluid film squeezed between two parallel plane surfaces”, *Journal of Fluid Mechanics* , Vol. 109, pp. 147-160.
- [15] Hayat, T. , Qayyum, A. and Alsaedi, A. (2015), “Three-dimensional mixed convection squeezing flow”, *Applied Mathematics and Mechanics – English Edition.* , Vol. 36 No. 1, pp. 47-60.
- [16] Jafarunnisa, S : Transient double diffusive flow of a viscous fluid with radiation effect in channels/Ducts, Ph.D Thesis, S.K.University, Anantapur, India (2011).
- [17] Jayasudha J.S. and Siva Prasad R : “Soret and Dufour effect on convective heat and mass transfer flow past a vertical porous plate in a rotating fluid with chemical reaction, radiation absorption and dissipation”, Ph.D. Thesis, Sri Krishnadevaraya University, Anantapuramu (2017)
- [18] Kuznetsov A.V., Nield D.A. : Natural convective boundary layer flow of a nanofluid past a vertical plate, *Int. J. Therm. Sci.* V.49, pp.243–247, (2010).
- [19] Madhavilatha, S and Prasada rao, D.R.V: Finite element analysis of convective heat and mass transfer flow past a vertical porous plate in a rotating fluid., *Int. Jour. Emerging and development*, Vol.3, pp.202-216, (2017)
- [20] Mahajan A and Arora M. : Convection in rotating magnetic nanofluids. *Applied Mathematics and Computation*; V.219: pp. 6284–6296(2013).
- [21] Mahanthesh B, Gorla R S R, Gireesha B J : “Mixed convection squeezing three-dimensional flow in a rotating channel filled with nanofluid”, *International Journal of Numerical Methods for Heat & Fluid flow*, Vol.26, Issue 5 pp.1460-1485(2016)
- [22] Munawar, S. , Mehmood, A. and Ali, A. (2012), “Three-dimensional squeezing flow in a rotating channel of lower stretching porous wall”, *Computers and Mathematics with Applications* , Vol. 64 No. 6, pp. 1575-1586.
- [23] Mustafa, M. , Hayat, T. and Obaidat, S. (2012), “On heat and mass transfer in the unsteady squeezing flow between parallel plates”, *Meccanica* , Vol. 47 No. 7, pp. 1581-1589.
- [24] Muthu kumaraswamy R., Senthil G.K. : Heat and mass transfer effects on moving vertical plate in the presence of thermal radiation, *Theor. Appl. Mach.* Pp. 35–46(2014).
- [25] Nadeem S and Saleem S. : Unsteady mixed convection flow of nanofluid on a rotating cone with magnetic field. *Appl. Nanoscience*; V.4: pp.405-414(2014).

- [26] Rana P, Bhargava R and Beg O.A. : Finite element simulation of unsteady magnetohydrodynamic transport phenomena on a stretching sheet in a rotating nanofluid. *Proc. I Mech. E- Part N: J. Nano materials, Nanoengineering and Nanosystems*, V.227: pp.77–99(2013).
- [27] Sheikholeslami M, Hatami M and Ganji DD. : Nanofluid flow and heat transfer in a rotating system in the presence of a magnetic field. *J. Molecular Liquids*; V.190: pp.112–120 (2014).
- [28] Sheikholeslami M., Ganji D.D. : Magnetohydrodynamic flow in a permeable channel filled with nanofluid, *Sci. Iran*, V.21 (1) , pp. 203–212 (2014).
- [29] Sheikholeslami M., Ganji D.D. : Unsteady nanofluid flow and heat transfer in presence of magnetic field considering thermal radiation, *J. Braz. Soc. Mech. Sci. Eng.* <http://dx.doi.org/10.1007/s40430-014-0228-x>.
- [30] Sreerangavani,K, Rajeswara Rao,U and Prasada Rao,D.R.V:Effect of thermo-diffusion on Mhd convection heat and mass transfer flow of chemically reacting fluid through a porous medium in a rotating system.,Presented in 2<sup>nd</sup> International conference on Applications of Fluid dynamics,July,(2014)
- [31] Sreevani,M : Mixed convective heat and mass transfer through a porous medium in channels with dissipative effects, Ph.D thesis, S.K.University, Anantapur , India (2002).
- [32] Stefan, M.J. (1874), “Versuch U ber die scheinbare adhesion Sitzungsberichte der Akademie der Wissenschaften in Wien”, *Mathematik-Naturwissen* , Vol. 69, pp. 713-721.
- [33] Sukanya J.S and Leelarathnam A : “Combined influence of Hall Currents and Soret effect on convective heat and mass transfer flow past vertical porous stretching plate in rotating fluid and dissipation with constant heat and mass flux and partial slip”, *IJATED* (2018)
- [34] Turkyilmazoglu M. : Exact analytical solutions for heat and mass transfer of MHD slip flow in nanofluids, *Chem. Eng. Sci.*, V.84, pp.182–187 (2014).
- [35] Turkyilmazoglu M., Pop I. : Heat and mass transfer of unsteady natural convection flow of some nanofluids past a vertical infinite flat plate with radiation effect, *Int. J. Heat Mass Transfer*, V.59, pp.167–171(2013).
- [36] Wang X, Xu X, Choi S.U.S. : Thermal conductivity of nanoparticle fluid mixture, *J. Thermophys. Heat Transfer*, V.13, pp.474–480(1999).
- [37] Zanchini, E : Effect of viscous dissipation on mixed convection in a vertical channel with boundary conditions of the third kind. *Int. J. of Heat and Mass Transfer*, V.41, pp.3949-3959 (1998).



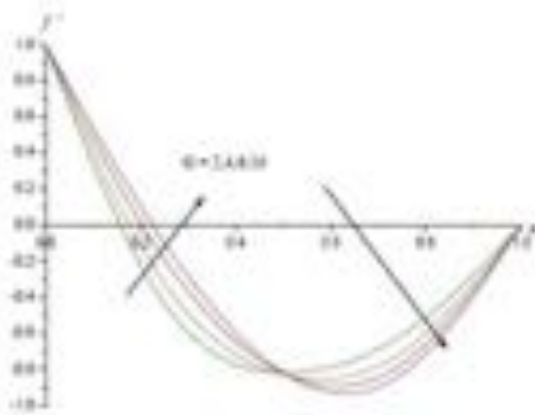


Fig. 2a Variation of  $f''$  with  $G$   
 $M=0.5, \mu=0.5, R=0.5, Q=0.5, Nr=0.5, \beta=0.2,$   
 $\phi=0.1, \gamma=0.5, Br=0.5, Sc=1.3, Qi=0.5, Pr=0.71$

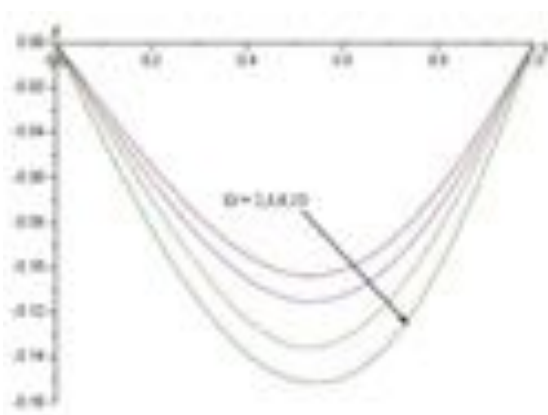


Fig. 2b Variation of  $g$  with  $G$   
 $M=0.5, \mu=0.5, R=0.5, Q=0.5, Nr=0.5, \beta=0.2,$   
 $\phi=0.1, \gamma=0.5, Br=0.5, Sc=1.3, Qi=0.5, Pr=0.71$

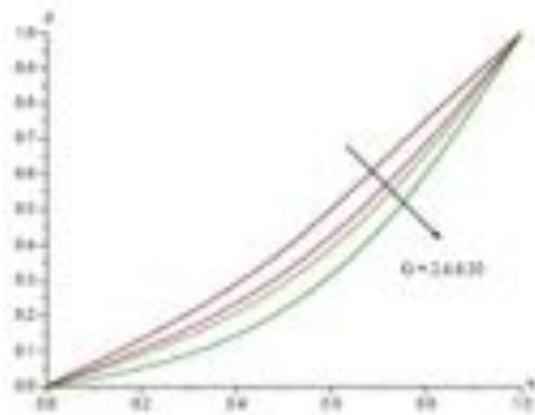


Fig. 2c Variation of  $P$  with  $G$   
 $M=0.5, \mu=0.5, R=0.5, Q=0.5, Nr=0.5, \beta=0.2,$   
 $\phi=0.1, \gamma=0.5, Br=0.5, Sc=1.3, Qi=0.5, Pr=0.71$

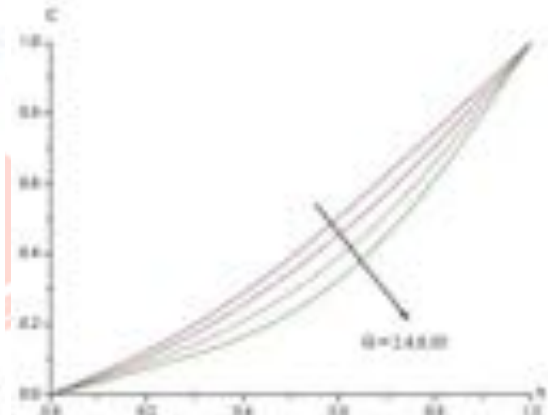


Fig. 2d Variation of  $C$  with  $G$   
 $M=0.5, \mu=0.5, R=0.5, Q=0.5, Nr=0.5, \beta=0.2,$   
 $\phi=0.1, \gamma=0.5, Br=0.5, Sc=1.3, Qi=0.5, Pr=0.71$

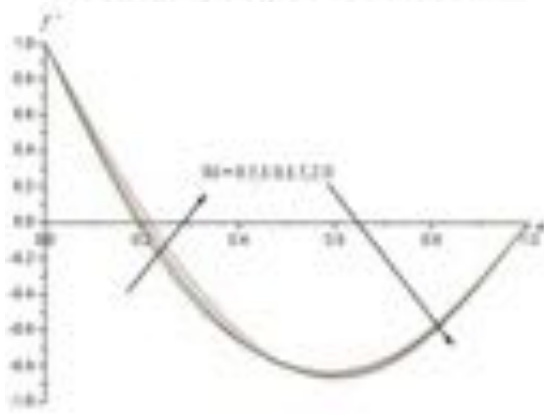


Fig. 3a Variation of  $f''$  with  $M$   
 $G=2, \mu=0.5, R=0.5, Q=0.5, Nr=0.5, \beta=0.2,$   
 $\phi=0.1, \gamma=0.5, Br=0.5, Sc=1.3, Qi=0.5, Pr=0.71$

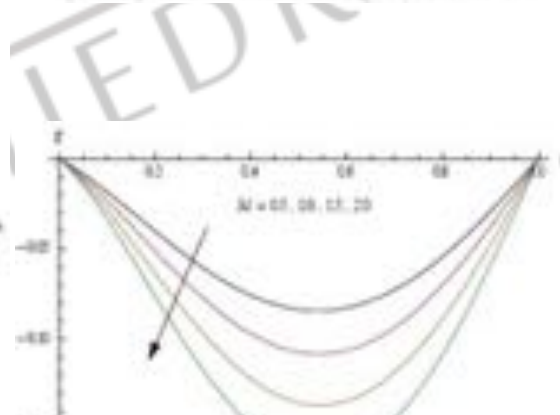


Fig. 3b Variation of  $g$  with  $M$   
 $G=2, \mu=0.5, R=0.5, Q=0.5, Nr=0.5, \beta=0.2,$   
 $\phi=0.1, \gamma=0.5, Br=0.5, Sc=1.3, Qi=0.5, Pr=0.71$

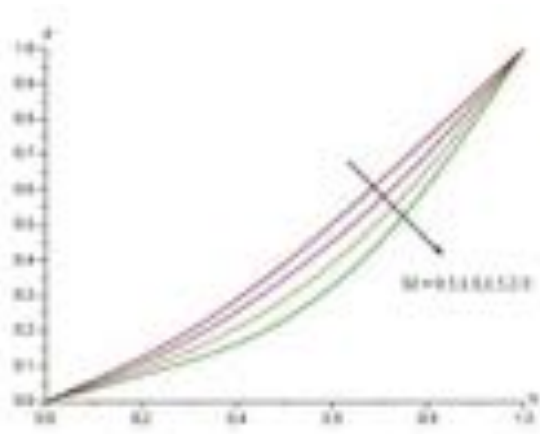


Fig. 3c Variation of  $\phi$  with  $M$   
 $G=2, m=0.5, R=0.5, Q=0.5, Nr=0.5, \beta=0.2,$   
 $\phi=0.1, \gamma=0.5, fw=0.5, Sc=1.3, Q1=0.5, Pr=0.71$

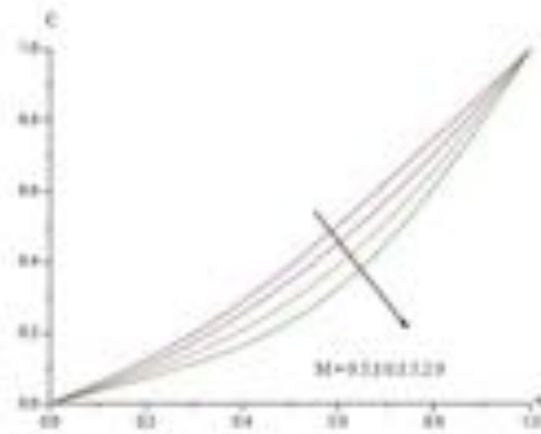


Fig. 3d Variation of  $C$  with  $M$   
 $G=2, m=0.5, R=0.5, Q=0.5, Nr=0.5, \beta=0.2,$   
 $\phi=0.1, \gamma=0.5, fw=0.5, Sc=1.3, Q1=0.5, Pr=0.71$

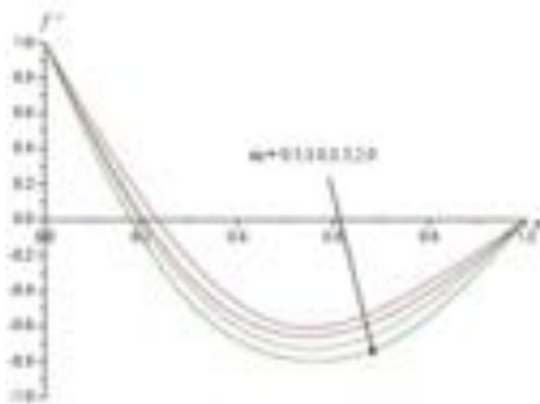


Fig. 4a Variation of  $f''$  with  $m$   
 $G=2, M=0.5, R=0.5, Q=0.5, Nr=0.5, \beta=0.2,$   
 $\phi=0.1, \gamma=0.5, fw=0.5, Sc=1.3, Q1=0.5, Pr=0.71$

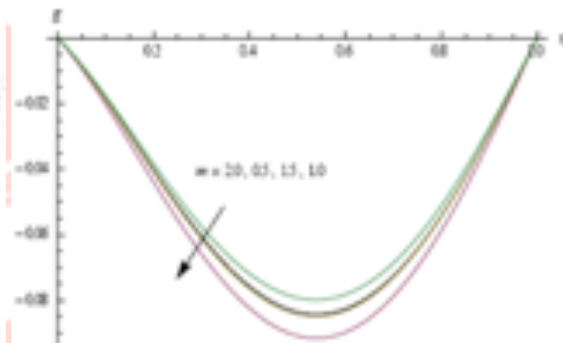


Fig. 4b Variation of  $g$  with  $m$   
 $G=2, M=0.5, R=0.5, Q=0.5, Nr=0.5, \beta=0.2,$   
 $\phi=0.1, \gamma=0.5, fw=0.5, Sc=1.3, Q1=0.5, Pr=0.71$

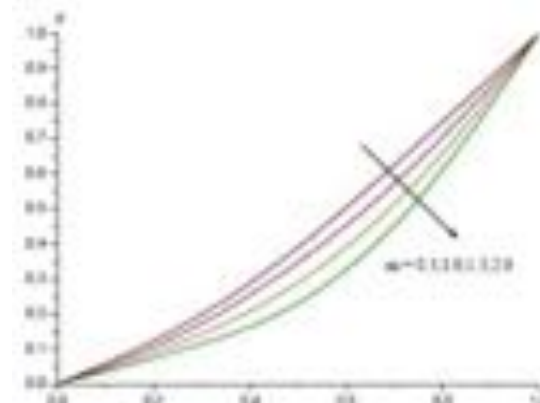


Fig. 4c Variation of  $\phi$  with  $m$   
 $G=2, M=0.5, R=0.5, Q=0.5, Nr=0.5, \beta=0.2,$   
 $\phi=0.1, \gamma=0.5, fw=0.5, Sc=1.3, Q1=0.5, Pr=0.71$

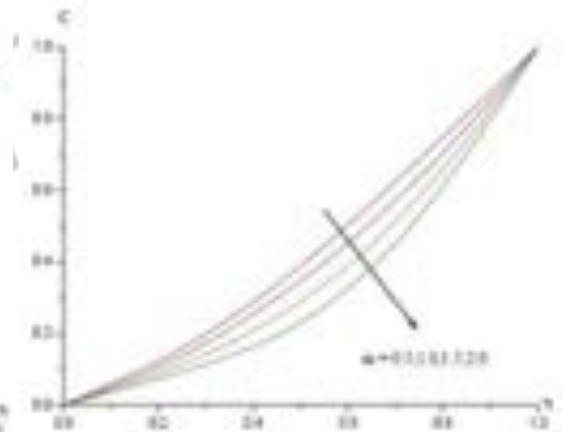


Fig. 4d Variation of  $C$  with  $m$   
 $G=2, M=0.5, R=0.5, Q=0.5, Nr=0.5, \beta=0.2,$   
 $\phi=0.1, \gamma=0.5, fw=0.5, Sc=1.3, Q1=0.5, Pr=0.71$

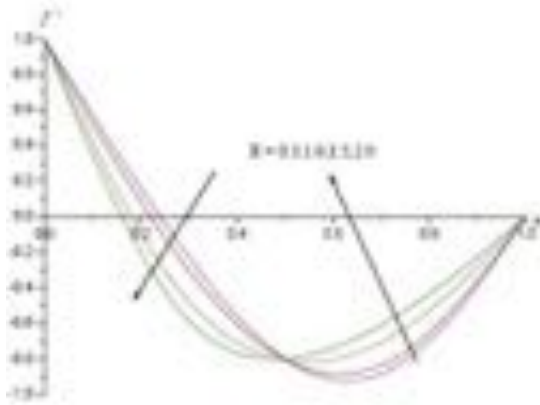


Fig. 5a Variation of  $f''$  with  $R$   
 $G=2, M=0.5, \mu=0.5, Q=0.5, Nr=0.5, \beta=0.2,$   
 $\phi=0.1, \gamma=0.5, Br=0.5, Sc=1.3, Qi=0.5, Pr=0.71$

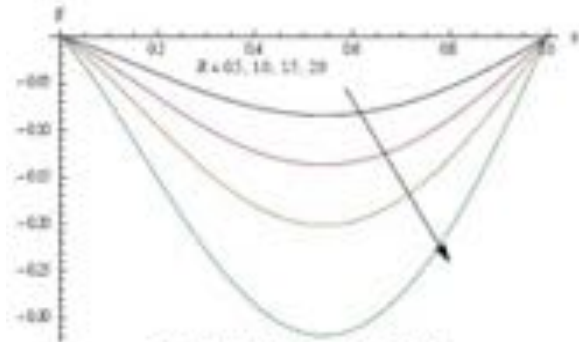


Fig. 5b Variation of  $g$  with  $R$   
 $G=2, M=0.5, \mu=0.5, Q=0.5, Nr=0.5, \beta=0.2,$   
 $\phi=0.1, \gamma=0.5, Br=0.5, Sc=1.3, Qi=0.5, Pr=0.71$

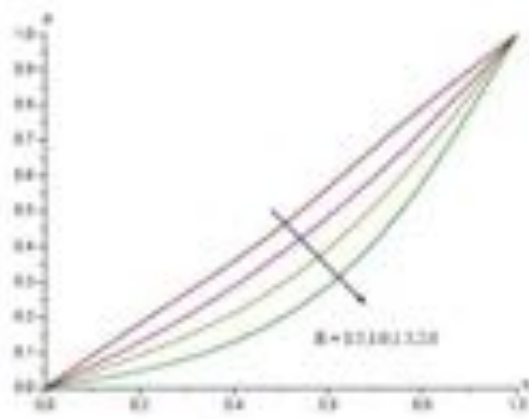


Fig. 5c Variation of  $d$  with  $R$   
 $G=2, M=0.5, \mu=0.5, Q=0.5, Nr=0.5, \beta=0.2,$   
 $\phi=0.1, \gamma=0.5, Br=0.5, Sc=1.3, Qi=0.5, Pr=0.71$

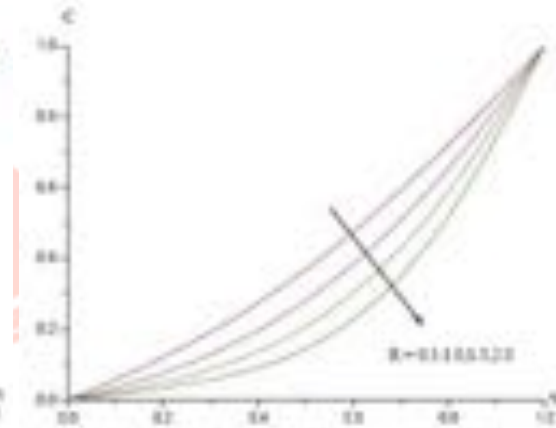


Fig. 5d Variation of  $C$  with  $R$   
 $G=2, M=0.5, \mu=0.5, Q=0.5, Nr=0.5, \beta=0.2,$   
 $\phi=0.1, \gamma=0.5, Br=0.5, Sc=1.3, Qi=0.5, Pr=0.71$

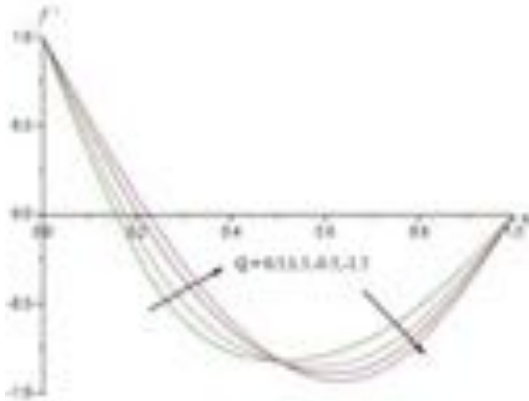


Fig. 6a Variation of  $f''$  with  $Q$   
 $G=2, M=0.5, \mu=0.5, R=0.5, Nr=0.5, \beta=0.2,$   
 $\phi=0.1, \gamma=0.5, Br=0.5, Sc=1.3, Qi=0.5, Pr=0.71$

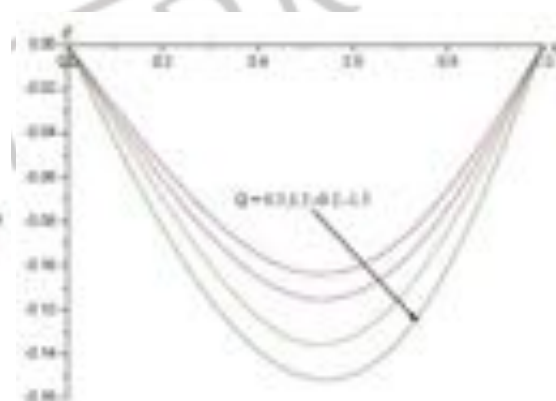
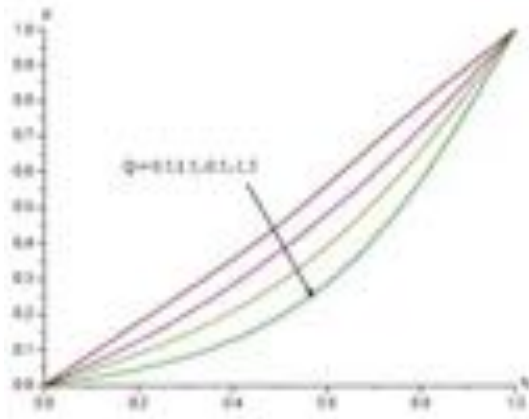
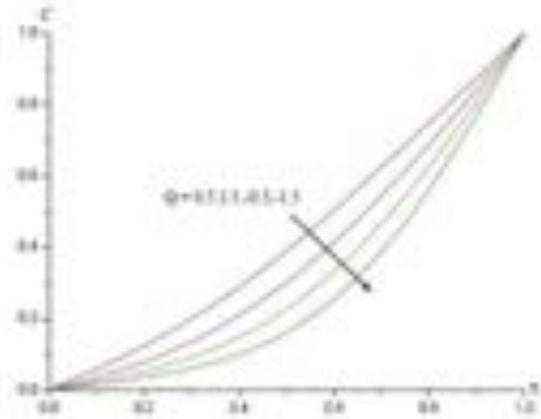


Fig. 6b Variation of  $g$  with  $Q$   
 $G=2, M=0.5, \mu=0.5, R=0.5, Nr=0.5, \beta=0.2,$   
 $\phi=0.1, \gamma=0.5, Br=0.5, Sc=1.3, Qi=0.5, Pr=0.71$



**Fig.6c Variation of  $\beta$  with Q**  
 $G=2, M=0.5, \mu=0.5, R=0.5, N_r=0.5, \beta=0.2,$   
 $\phi=0.1, \gamma=0.5, \delta_r=0.5, S_c=1.3, Q_1=0.5, P_r=0.71$



**Fig.6d Variation of C with Q**  
 $G=2, M=0.5, \mu=0.5, R=0.5, N_r=0.5, \beta=0.2,$   
 $\phi=0.1, \gamma=0.5, \delta_r=0.5, S_c=1.3, Q_1=0.5, P_r=0.71$

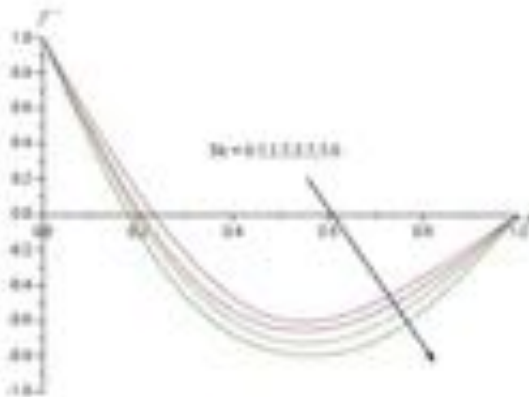


**Fig.7a Variation of  $f'$  with  $N_r$**   
 $G=2, M=0.5, \mu=0.5, R=0.5, Q=0.5, \beta=0.2,$   
 $\phi=0.1, \gamma=0.5, \delta_r=0.5, S_c=1.3, Q_1=0.5, P_r=0.71$

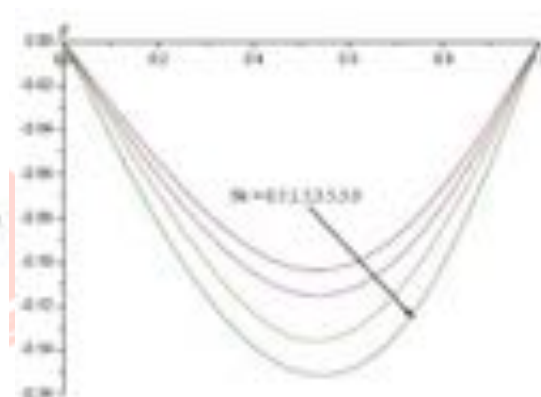


**Fig.7b Variation of g with  $N_r$**   
 $G=2, M=0.5, \mu=0.5, R=0.5, Q=0.5, \beta=0.2,$   
 $\phi=0.1, \gamma=0.5, \delta_r=0.5, S_c=1.3, Q_1=0.5, P_r=0.71$

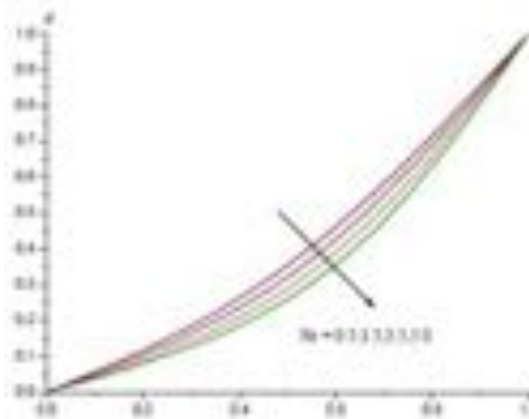


**Fig.7c Variation of  $\theta$  with  $N_r$**   
 $G=2, M=0.5, \mu=0.5, R=0.5, Q=0.5, \beta=0.2,$   
 $\phi=0.1, \gamma=0.5, \delta_r=0.5, S_c=1.3, Q_1=0.5, P_r=0.71$

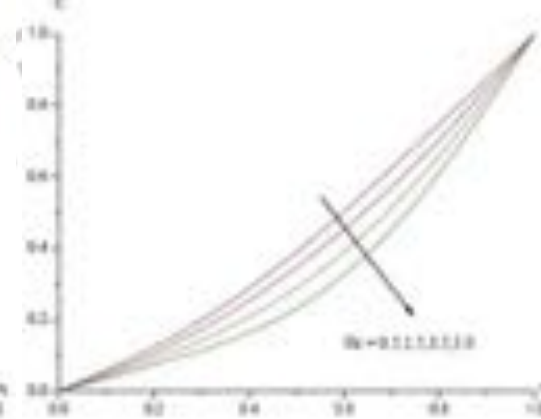


**Fig.7d Variation of C with  $N_r$**   
 $G=2, M=0.5, \mu=0.5, R=0.5, Q=0.5, \beta=0.2,$   
 $\phi=0.1, \gamma=0.5, \delta_r=0.5, S_c=1.3, Q_1=0.5, P_r=0.71$

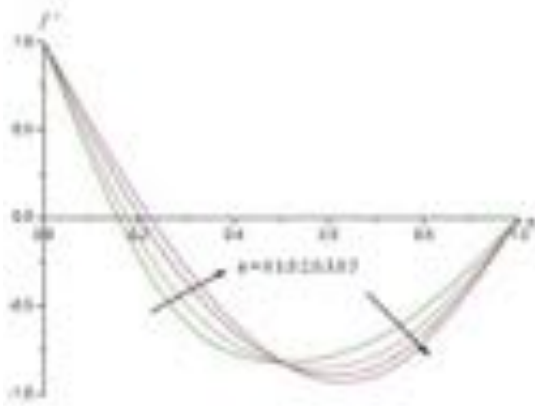


Fig.8a Variation of  $f''$  with  $\phi$   
 $G=2, M=0.5, \mu=0.5, R=0.5, Q=0.5, N_r=0.5, \beta=0.2,$   
 $\gamma=0.5, f_w=0.5, S_c=1.3, Q_1=0.5, Pr=0.71$

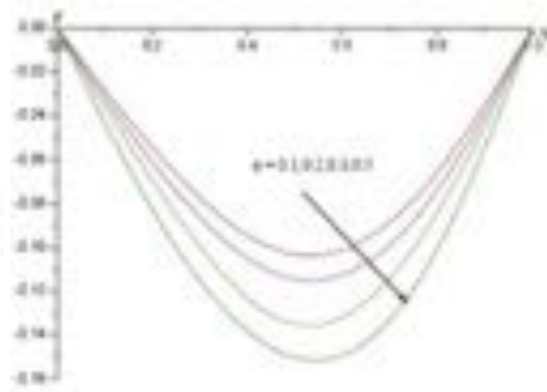


Fig.8b Variation of  $g$  with  $\phi$   
 $G=2, M=0.5, \mu=0.5, R=0.5, Q=0.5, N_r=0.5, \beta=0.2,$   
 $\gamma=0.5, f_w=0.5, S_c=1.3, Q_1=0.5, Pr=0.71$

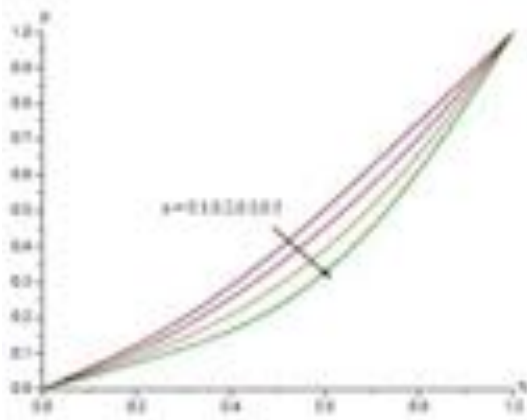


Fig.8c Variation of  $\theta$  with  $\phi$   
 $G=2, M=0.5, \mu=0.5, R=0.5, Q=0.5, N_r=0.5, \beta=0.2,$   
 $\gamma=0.5, f_w=0.5, S_c=1.3, Q_1=0.5, Pr=0.71$

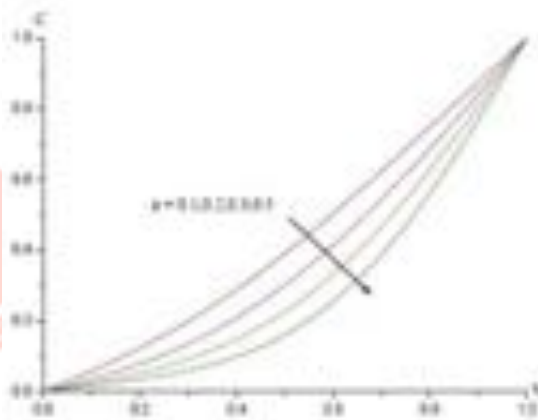


Fig.8d Variation of  $C$  with  $\phi$   
 $G=2, M=0.5, \mu=0.5, R=0.5, Q=0.5, N_r=0.5, \beta=0.2,$   
 $\gamma=0.5, f_w=0.5, S_c=1.3, Q_1=0.5, Pr=0.71$

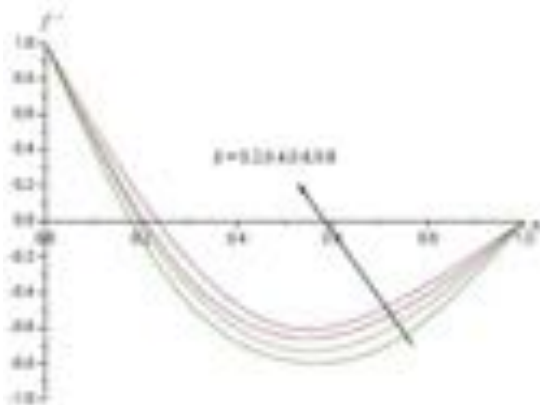


Fig.9a Variation of  $f''$  with  $\beta$   
 $G=2, M=0.5, \mu=0.5, R=0.5, Q=0.5, N_r=0.5, \gamma=0.5,$   
 $\phi=0.1, f_w=0.5, S_c=1.3, Q_1=0.5, Pr=0.71$

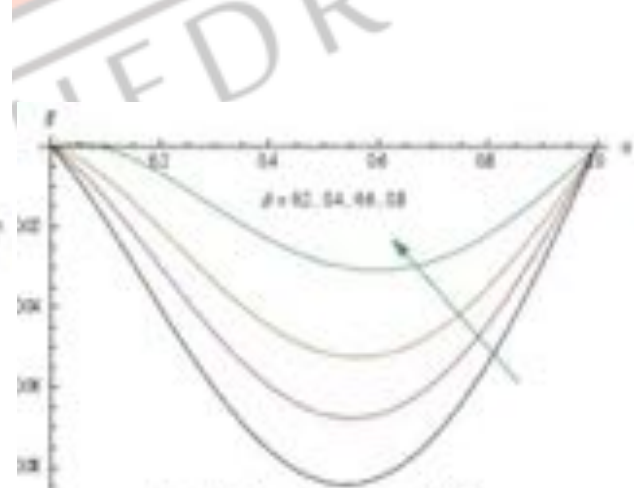


Fig.9b Variation of  $g$  with  $\beta$   
 $G=2, M=0.5, \mu=0.5, R=0.5, Q=0.5, N_r=0.5, \gamma=0.5,$   
 $\phi=0.1, f_w=0.5, S_c=1.3, Q_1=0.5, Pr=0.71$



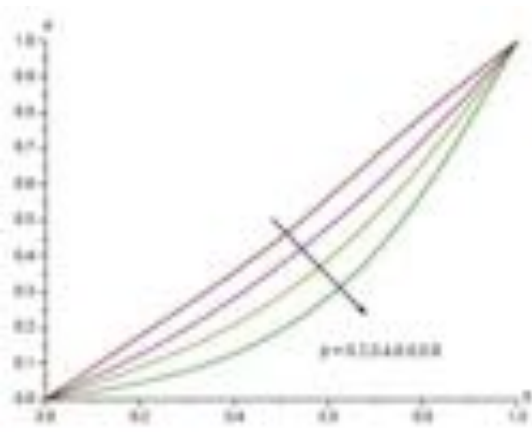


Fig. 9c Variation of  $\theta$  with  $\beta$   
 $G=2, M=0.5, \mu=0.5, R=0.5, Q=0.5, N_1=0.5,$   
 $\gamma=0.5, \phi=0.1, Sc=1.3, Q_1=0.5, Pr=0.71$

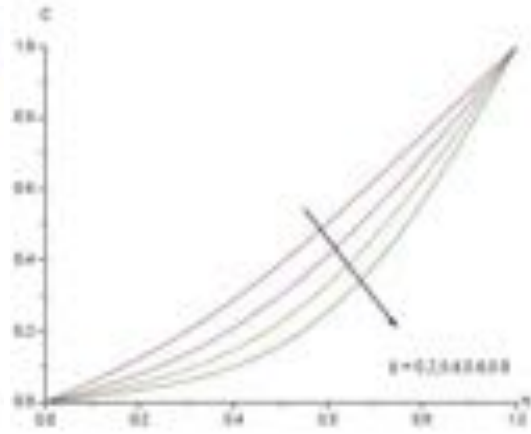


Fig. 9d Variation of  $C$  with  $\beta$   
 $G=2, M=0.5, \mu=0.5, R=0.5, Q=0.5, N_1=0.5, \gamma=0.5,$   
 $\phi=0.1, Sc=1.3, Q_1=0.5, Pr=0.71$

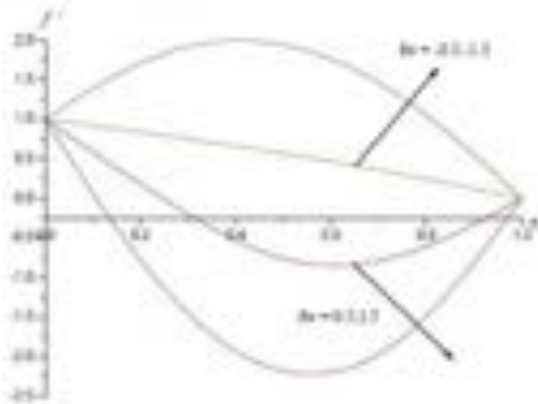


Fig. 10a Variation of  $f'$  with  $\beta$   
 $G=2, M=0.5, \mu=0.5, R=0.5, Q=0.5, N_1=0.5, \beta=0.2,$   
 $\gamma=0.5, \phi=0.1, Sc=1.3, Q_1=0.5, Pr=0.71$

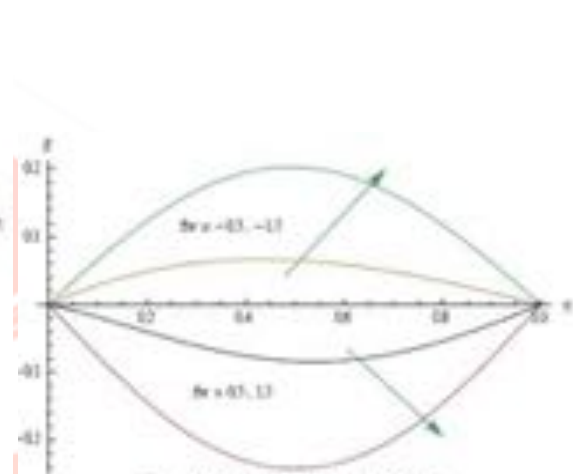


Fig. 10b Variation of  $g$  with  $\beta$   
 $G=2, M=0.5, \mu=0.5, R=0.5, Q=0.5, N_1=0.5, \beta=0.2,$   
 $\gamma=0.5, \phi=0.1, Sc=1.3, Q_1=0.5, Pr=0.71$

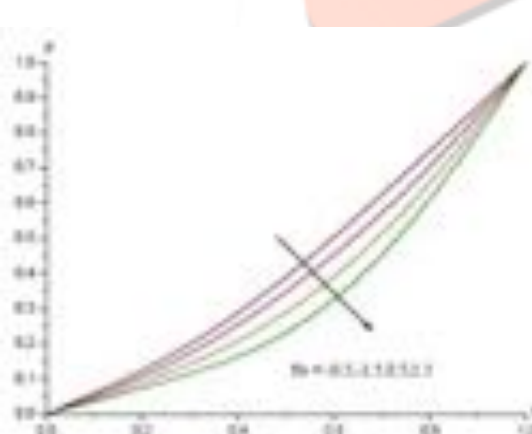


Fig. 10c Variation of  $\theta$  with  $\beta$   
 $G=2, M=0.5, \mu=0.5, R=0.5, Q=0.5, N_1=0.5, \beta=0.2,$   
 $\gamma=0.5, \phi=0.1, Sc=1.3, Q_1=0.5, Pr=0.71$

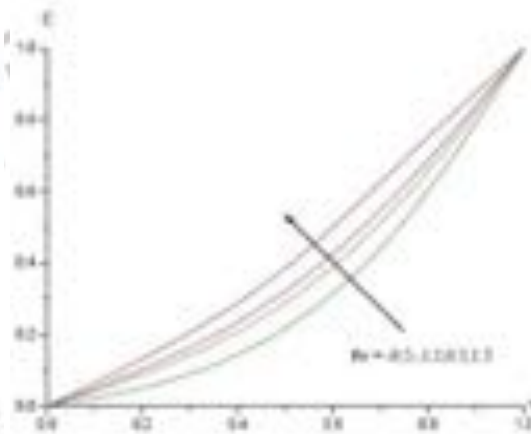


Fig. 10d Variation of  $C$  with  $\beta$   
 $G=2, M=0.5, \mu=0.5, R=0.5, Q=0.5, N_1=0.5, \beta=0.2,$   
 $\gamma=0.5, \phi=0.1, Sc=1.3, Q_1=0.5, Pr=0.71$

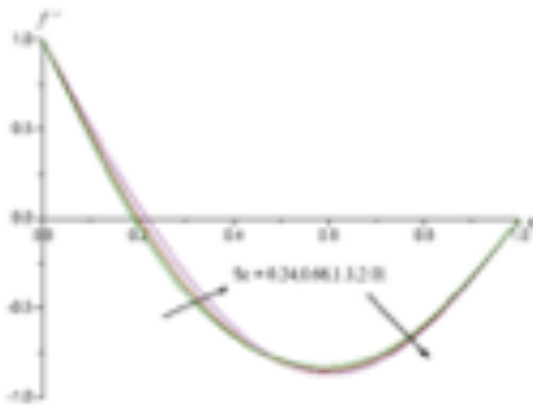


Fig. 11a Variation of  $f'$  with  $Sc$   
 $G=2, M=0.5, \mu=0.5, R=0.5, Q=0.5, N_r=0.5, \beta=0.2,$   
 $\gamma=0.5, \phi=0.1, \rho=0.5, Q_1=0.5, Pr=0.71$

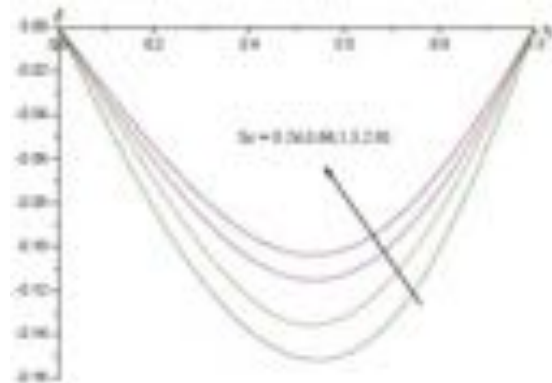


Fig. 11b Variation of  $g$  with  $Sc$   
 $G=2, M=0.5, \mu=0.5, R=0.5, Q=0.5, N_r=0.5, \beta=0.2,$   
 $\gamma=0.5, \phi=0.1, \rho=0.5, Q_1=0.5, Pr=0.71$

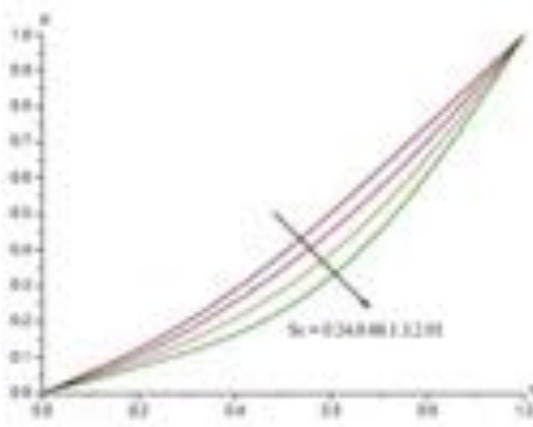


Fig. 11c Variation of  $\theta$  with  $Sc$   
 $G=2, M=0.5, \mu=0.5, R=0.5, Q=0.5, N_r=0.5, \beta=0.2,$   
 $\gamma=0.5, \phi=0.1, \rho=0.5, Q_1=0.5, Pr=0.71$

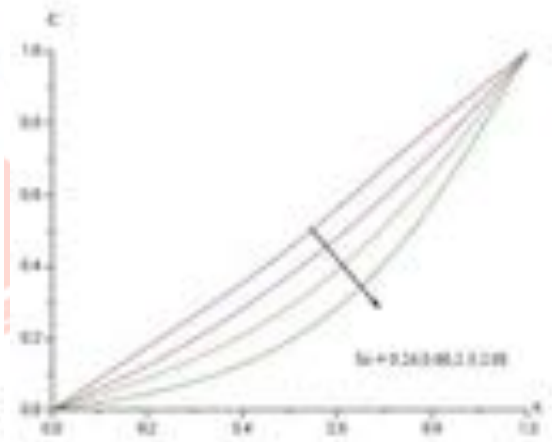


Fig. 11d Variation of  $C$  with  $Sc$   
 $G=2, M=0.5, \mu=0.5, R=0.5, Q=0.5, N_r=0.5, \beta=0.2,$   
 $\gamma=0.5, \phi=0.1, \rho=0.5, Q_1=0.5, Pr=0.71$

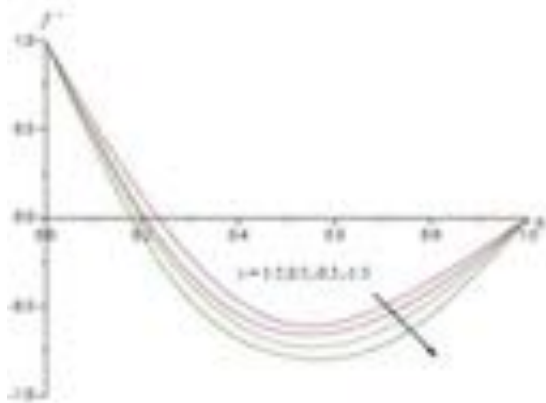


Fig. 12a Variation of  $f'$  with  $\gamma$   
 $G=2, M=0.5, \mu=0.5, R=0.5, Q=0.5, N_r=0.5, \beta=0.2,$   
 $\phi=0.1, \rho=0.5, Sc=1.3, Q_1=0.5, Pr=0.71$

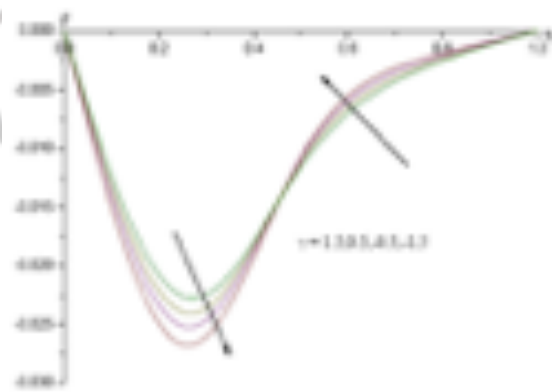


Fig. 12b Variation of  $g$  with  $\gamma$   
 $G=2, M=0.5, \mu=0.5, R=0.5, Q=0.5, N_r=0.5, \beta=0.2,$   
 $\phi=0.1, \rho=0.5, Sc=1.3, N_r=0.5, Q_1=0.5, Pr=0.71$

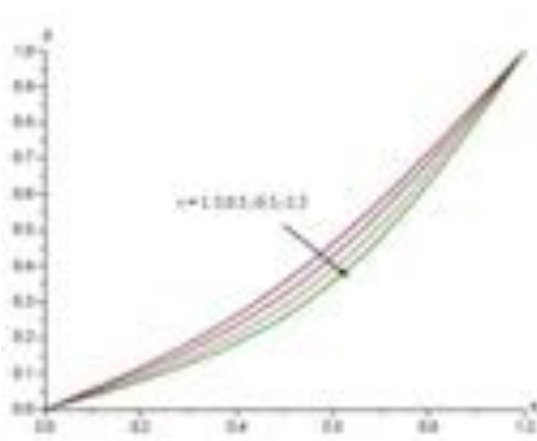


Fig. 12a Variation of  $\theta$  with  $\gamma$   
 $G=2.5, M=0.5, \alpha=0.5, R=0.5, Q=0.5, N=0.5, \beta=0.2,$   
 $\phi=0.1, f=0.5, Sc=1.3, Qi=0.5, Pr=0.71$

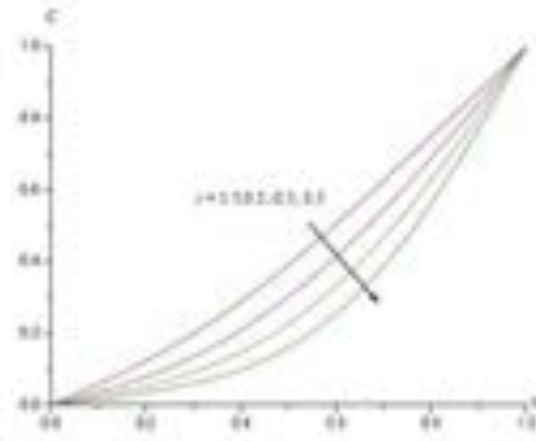


Fig. 12b Variation of  $C$  with  $\gamma$   
 $G=2.5, M=0.5, \alpha=0.5, R=0.5, Q=0.5, N=0.5, \beta=0.2,$   
 $\phi=0.1, f=0.5, Sc=1.3, Qi=0.5, Pr=0.71$

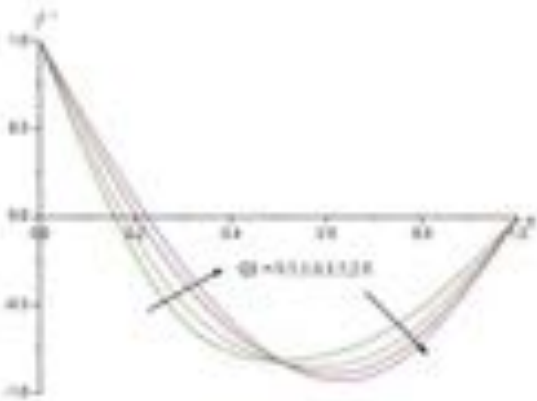


Fig. 13a Variation of  $f'$  with  $Qi$   
 $G=2.5, M=0.5, \alpha=0.5, R=0.5, Q=0.5, N=0.5, \beta=0.2,$   
 $\gamma=0.5, \phi=0.1, f=0.5, Sc=1.3, Pr=0.71$

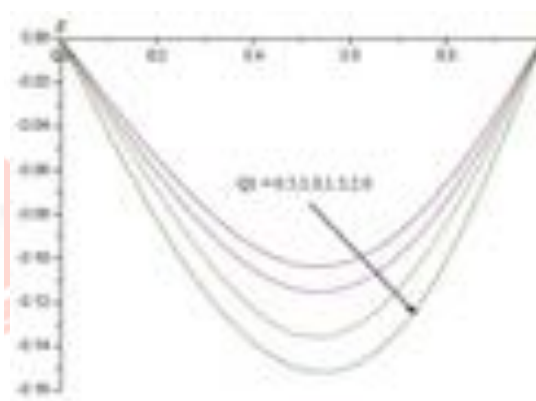


Fig. 13b Variation of  $g$  with  $Qi$   
 $G=2.5, M=0.5, \alpha=0.5, R=0.5, Q=0.5, N=0.5, \beta=0.2,$   
 $\gamma=0.5, \phi=0.1, f=0.5, Sc=1.3, Pr=0.71$

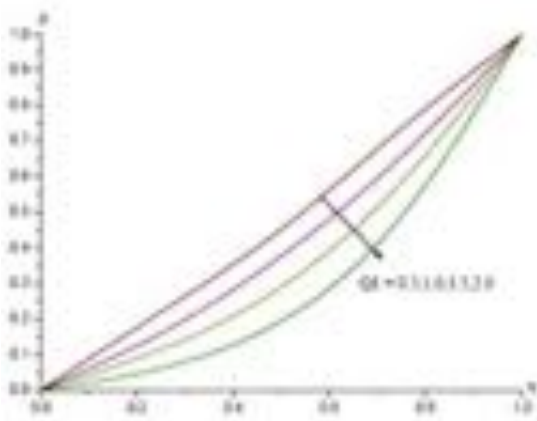


Fig. 13c Variation of  $\theta$  with  $Qi$   
 $G=2.5, M=0.5, \alpha=0.5, R=0.5, Q=0.5, N=0.5, \beta=0.2,$   
 $\gamma=0.5, \phi=0.1, f=0.5, Sc=1.3, Pr=0.71$

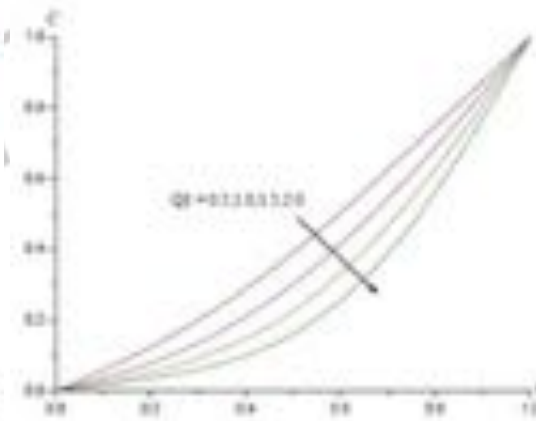


Fig. 13d Variation of  $C$  with  $Qi$   
 $G=2.5, M=0.5, \alpha=0.5, R=0.5, Q=0.5, N=0.5, \beta=0.2,$   
 $\gamma=0.5, \phi=0.1, f=0.5, Sc=1.3, Pr=0.71$

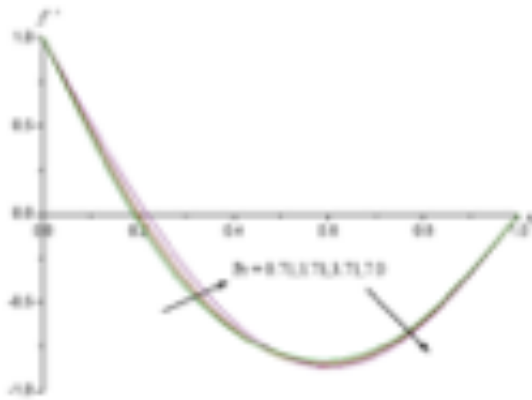


Fig.14a Variation of  $f''$  with  $Pr$   
 $G=2, M=0.5, \alpha=0.5, R=0.5, Q=0.5, N=0.5, \beta=0.2,$   
 $\gamma=0.5, \phi=0.1, f_w=0.5, Sc=1.3, Q1=0.5$

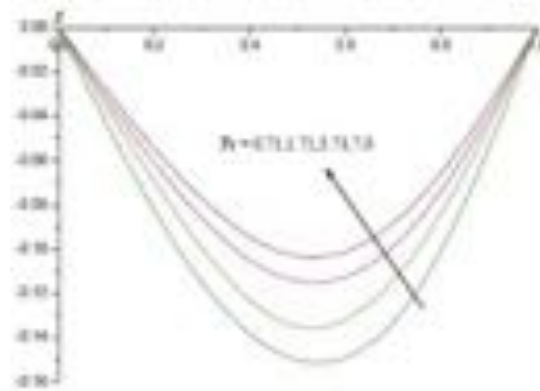


Fig.14b Variation of  $g$  with  $Pr$   
 $G=2, M=0.5, \alpha=0.5, R=0.5, Q=0.5, N=0.5, \beta=0.2,$   
 $\gamma=0.5, \phi=0.1, f_w=0.5, Sc=1.3, Q1=0.5$

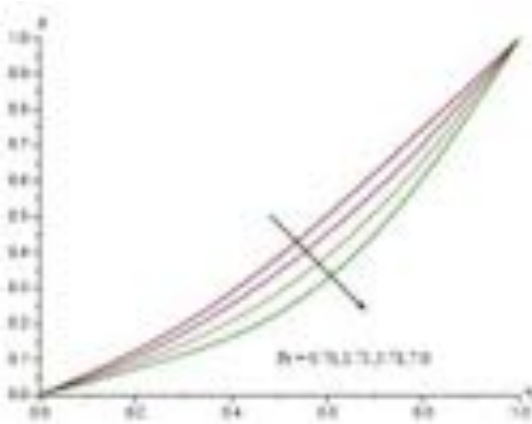


Fig.14c Variation of  $\phi$  with  $Pr$   
 $G=2, M=0.5, \alpha=0.5, R=0.5, Q=0.5, N=0.5, \beta=0.2,$   
 $\gamma=0.5, \phi=0.1, f_w=0.5, Sc=1.3, Q1=0.5$

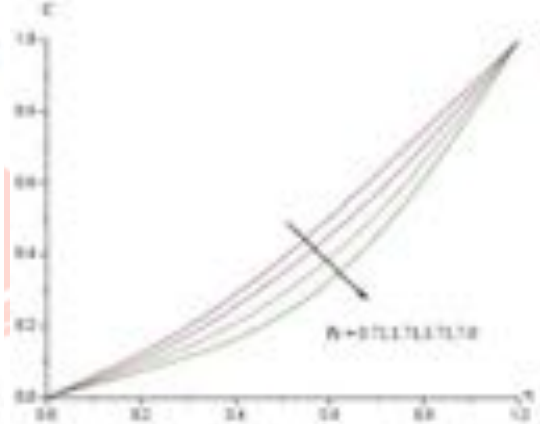


Fig.14d Variation of  $C$  with  $Pr$   
 $G=2, M=0.5, \alpha=0.5, R=0.5, Q=0.5, N=0.5, \beta=0.2,$   
 $\gamma=0.5, \phi=0.1, f_w=0.5, Sc=1.3, Q1=0.5$



**Table 2 : Skin friction( $\tau_x, \tau_z$ ), Nusselt Number (Nu) and Sherwood Number (Sh) at  $\eta=0\&1$**

| Parameter                  |             | $\eta = 0 \& 1$ |             |             |             |            |           |           |          |
|----------------------------|-------------|-----------------|-------------|-------------|-------------|------------|-----------|-----------|----------|
|                            |             | $\tau_x(0)$     | $\tau_x(1)$ | $\tau_z(0)$ | $\tau_z(1)$ | Nu(0)      | Nu(1)     | Sh(0)     | Sh(1)    |
| <b>G</b>                   | <b>2</b>    | -6.55624        | 4.85589     | -0.147492   | 0.297567    | -0.999818  | -1.0003   | -0.638442 | -1.42411 |
|                            | <b>4</b>    | -6.58134        | 4.81623     | -0.147562   | 0.297025    | -0.999193  | -1.00062  | -0.639401 | -1.42319 |
|                            | <b>6</b>    | -6.60656        | 4.77652     | -0.148212   | 0.296481    | -0.999635  | -1.00069  | -0.639106 | -1.42299 |
|                            | <b>10</b>   | -6.65694        | 4.69716     | -0.149172   | 0.295397    | -0.998651  | -1.00076  | -0.640648 | -1.42211 |
| <b>M</b>                   | <b>0.5</b>  | -6.55624        | 4.85589     | -0.147492   | 0.297567    | -0.999818  | -1.00031  | -0.638441 | -1.42411 |
|                            | <b>1.0</b>  | -6.69248        | 4.86372     | -0.174599   | 0.384182    | -0.999193  | -1.00018  | -0.639732 | -1.42344 |
|                            | <b>1.5</b>  | -6.88193        | 4.87746     | -0.210114   | 0.488215    | -0.999636  | -1.00039  | -0.639972 | -1.42247 |
|                            | <b>2.0</b>  | -7.41083        | 4.93033     | -0.245556   | 0.708624    | -0.998654  | -1.00129  | -0.643107 | -1.41942 |
| <b>m</b>                   | <b>0.5</b>  | -6.55624        | 4.85589     | -0.147492   | 0.297567    | -0.999818  | -1.00031  | -0.638442 | -1.42411 |
|                            | <b>1.0</b>  | -6.48957        | 4.85335     | -0.163783   | 0.322661    | -0.999792  | -1.00019  | -0.638878 | -1.42428 |
|                            | <b>1.5</b>  | -6.46601        | 4.85221     | -0.152261   | 0.298916    | -0.999634  | -1.00035  | -0.639241 | -1.42484 |
|                            | <b>2.0</b>  | -6.45725        | 4.85177     | -0.141458   | 0.281008    | -0.998649  | -1.00127  | -0.639466 | -1.42307 |
| <b>R</b>                   | <b>0.5</b>  | -6.55624        | -6.55616    | -0.147492   | -0.147052   | -0.999818  | -1.00035  | -0.638442 | -1.42411 |
|                            | <b>1.0</b>  | -6.54737        | -6.54737    | -0.228971   | -0.238971   | -0.999193  | -1.00006  | -0.639137 | -1.42409 |
|                            | <b>1.5</b>  | -6.52927        | -6.52927    | -0.301188   | -0.351188   | -0.998634  | -1.00003  | -0.639855 | -1.42579 |
|                            | <b>2.0</b>  | -6.47534        | -6.47534    | -0.534645   | -0.554645   | -0.998609  | -1.00129  | -0.639959 | -1.42273 |
| <b>Q</b>                   | <b>0.5</b>  | -6.55624        | 4.85589     | -0.147492   | 0.297567    | -0.999818  | -1.00031  | -0.638442 | -1.42407 |
|                            | <b>1.5</b>  | -6.55616        | 4.85599     | -0.147450   | 0.297562    | -0.999193  | -1.00029  | -0.639161 | -1.42422 |
|                            | <b>-0.5</b> | -6.55611        | 4.85589     | -0.147368   | 0.297560    | -0.999634  | -1.00037  | -0.638626 | -1.42376 |
|                            | <b>-1.5</b> | -6.55608        | 4.855824    | -0.147232   | 0.297569    | -0.998649  | -1.00127  | -0.639687 | -1.42265 |
| <b>Nr</b>                  | <b>0.5</b>  | -6.55624        | 4.85589     | -0.147492   | 0.297567    | -0.999818  | -1.00213  | -0.638442 | -1.42411 |
|                            | <b>1.5</b>  | -6.55611        | 4.85595     | -0.147555   | 0.297568    | -0.997406  | -1.00311  | -0.636107 | -1.42522 |
|                            | <b>3.5</b>  | -6.55601        | 4.85601     | -0.147659   | 0.297570    | -0.996816  | -1.00349  | -0.635845 | -1.42621 |
|                            | <b>5.0</b>  | -6.55596        | 4.85555     | -0.147761   | 0.297576    | -0.991818  | -1.00538  | -0.647274 | -1.41758 |
| <b><math>\beta</math></b>  | <b>0.2</b>  | -6.55624        | 4.85589     | -0.147492   | 0.297567    | -0.999818  | -1.00031  | -0.638442 | -1.42411 |
|                            | <b>0.4</b>  | -5.90568        | 4.19969     | -0.087764   | 0.244442    | -0.998935  | -1.00072  | -0.583021 | -1.61207 |
|                            | <b>0.6</b>  | -5.29119        | 3.57964     | -0.0348215  | 0.195317    | -0.998666  | -1.00076  | -0.532381 | -1.79803 |
|                            | <b>0.8</b>  | -4.37863        | 2.65852     | 0.0307551   | 0.124204    | -0.998553  | -1.00111  | -0.465255 | -2.08516 |
| <b><math>\phi</math></b>   | <b>0.1</b>  | -6.55624        | 4.85589     | -0.147492   | 0.297567    | -0.999818  | -1.00031  | -0.927439 | -1.07491 |
|                            | <b>0.2</b>  | -6.61771        | 4.79723     | -0.0865207  | 0.200927    | -0.998722  | -1.00057  | -0.865878 | -1.14214 |
|                            | <b>0.3</b>  | -6.65563        | 4.75925     | -0.0531578  | 0.133882    | -0.99822   | -1.00069  | -0.927729 | -1.07475 |
|                            | <b>0.5</b>  | -6.69352        | 4.71654     | -0.0324464  | 0.0485352   | -0.998063  | -1.00091  | -0.928036 | -1.07455 |
| <b>fw</b>                  | <b>0.5</b>  | -6.55624        | 4.65589     | -0.147492   | 0.297567    | -0.999818  | -1.00031  | -0.927435 | -1.07491 |
|                            | <b>1.5</b>  | -11.7305        | 11.6962     | -0.749681   | 0.793682    | -0.997782  | -1.00106  | -0.741688 | -1.20604 |
|                            | <b>-0.5</b> | -0.72680        | -1.35245    | 0.339547    | -0.178573   | -1.00076   | -0.999385 | -1.001882 | -1.04232 |
|                            | <b>-1.5</b> | 5.91401         | -6.92129    | 0.585499    | -0.629888   | -1.00223   | -0.998863 | -1.079588 | -1.01091 |
| <b>Sc</b>                  | <b>0.24</b> | -6.55624        | 4.85592     | -0.1474952  | 0.297567    | -0.99984   | -1.00009  | -0.927431 | 1.074929 |
|                            | <b>0.66</b> | -6.55613        | 4.85593     | -0.147052   | 0.297567    | -0.998841  | -1.00037  | 0.865656  | 1.14243  |
|                            | <b>1.30</b> | -6.55614        | 4.85592     | -0.147052   | 0.297567    | -0.999364  | -0.999816 | -0.807902 | 1.20857  |
|                            | <b>2.01</b> | -6.55613        | 4.85593     | -0.147052   | 0.297567    | -0.998278  | -1.00039  | -0.729329 | 1.30556  |
| <b><math>\gamma</math></b> | <b>0.5</b>  | -6.55624        | 4.85589     | -0.147052   | 0.297567    | -0.99984   | -1.00009  | -0.927434 | -1.07502 |
|                            | <b>1.5</b>  | 6.55613         | 4.85593     | 0.147052    | 0.297567    | -0.998842  | 1.00039   | -0.894933 | -1.14621 |
|                            | <b>-0.5</b> | -6.55614        | 4.85592     | -0.147052   | 0.297567    | -0.999375  | -0.99980  | -0.961948 | -1.00231 |
|                            | <b>-1.5</b> | -6.55613        | 4.85593     | -0.147052   | 0.297567    | -0.998298  | -1.00040  | -0.998409 | -0.8995  |
| <b>Q1</b>                  | <b>0.5</b>  | -6.55624        | 4.85589     | -0.147152   | 0.297567    | -0.99984   | -1.0015   | -0.927431 | -1.07492 |
|                            | <b>1.0</b>  | -6.555523       | 4.85619     | -0.147222   | 0.297247    | -0.998956  | -1.0067   | -0.927621 | -1.07491 |
|                            | <b>1.5</b>  | -6.554518       | 4.85659     | -0.147342   | 0.296997    | -0.9982618 | -1.0083   | -0.927481 | -1.07509 |
|                            | <b>2.0</b>  | -6.553515       | 4.85722     | -0.147412   | 0.295567    | -0.99782   | -1.009156 | -0.927661 | -1.07507 |
| <b>Pr</b>                  | <b>0.71</b> | -6.55624        | 4.85589     | -0.147052   | 0.297567    | -0.999818  | -1.00011  | -0.927435 | -1.07496 |
|                            | <b>1.71</b> | -6.55603        | 4.85593     | -0.147049   | 0.297564    | -0.998737  | -1.00054  | -0.865691 | -1.14237 |
|                            | <b>3.71</b> | -6.55601        | 4.85588     | -0.147042   | 0.297556    | -0.999264  | -1.00113  | -0.927555 | -1.07496 |
|                            | <b>7</b>    | -6.55556        | 4.85579     | -0.147034   | 0.297545    | -0.999384  | -1.00059  | -0.928786 | -1.06489 |